Analysis of physical processes in eruptive YSOs with near-infrared spectra and multiwavelength light curves

Zhen Guo (郭震) [1]★ P. W. Lucas [1] C. Contreras Peña [1,2] L. C. Smith,[3] C. Morris,[1] R. G. Kurtev,[4,5]
J. Borissova [4,5] J. Alonso-García,[5,6] D. Minniti,[7,8] A.-N. Chené [9] M. S. N. Kumar,[10]
A. Caratti o Garatti,[11] D. Froebrich[12] and W. H. Stimson[1]

[1]*Centre for Astrophysics Research, University of Hertfordshire, Hatfield AL10 9AB, UK*
[2]*Department of Physics and Astronomy, University of Exeter, Stocker Road, Exeter, Devon EX4 4SB, UK*
[3]*Institute of Astronomy, University of Cambridge, Madingley Road, Cambridge CB3 0HA, UK*
[4]*Instituto de Física y Astronomía, Universidad de Valparaíso, Ave. Gran Bretaña 1111, Casilla 5030, Valparaíso, Chile*
[5]*Millennium Institute of Astrophysics, Santiago, 782-0436 Macul, Chile*
[6]*Centro de Astronomía (CITEVA), Universidad de Antofagasta, Av. Angamos 601, 02800 Antofagasta, Chile*
[7]*Departamento de Ciencias Fisicas, Universidad Andres Bello, Republica 220, 8320000 Santiago, Chile*
[8]*Vatican Observatory, V-00120 Vatican City State, Italy*
[9]*Gemini Observatory/NSF's NOIRLab, 670 N. A'ohoku Place, Hilo, HI 96720, USA*
[10]*Instituto de Astrofísica e Ciências do Espaco, Universidade do Porto, CAUP, Rua das Estrelas, P-4150-762 Porto, Portugal*
[11]*School of Cosmic Physics, Astronomy and Astrophysics Section, Dublin Institute for Advanced Studies, 31 Fitzwilliam Place, Dublin 2, Ireland*
[12]*Centre for Astrophysics and Planetary Science, School of Physical Sciences, University of Kent, Canterbury CT2 7NH, UK*

ABSTRACT

The decade-long Vista Variables in the Via Lactea (VVV) survey has detected numerous highly variable young stellar objects (YSOs). We present a study of 61 highly variable VVV YSOs ($\Delta K_s = 1$–5 mag), combining near-infrared spectra from Magellan and ESO Very Large Telescope with VVV and NEOWISE light curves to investigate physical mechanisms behind eruptive events. Most sources are spectroscopically confirmed as eruptive variables (typically Class I YSOs) but variable extinction is also seen. Among them, magnetically controlled accretion, identified by H I recombination emission (usually accompanied by CO emission), is observed in 46 YSOs. Boundary layer accretion, associated with FU Ori-like outbursts identified by CO overtone and H_2O absorption, is observed only in longer duration events (≥ 5 yr total duration). However, even in long duration events, the magnetically controlled accretion mode predominates, with amplitudes similar to the boundary layer mode. Shorter (100–700 d) eruptive events usually have lower amplitudes and these events are generally either periodic accretors or multiple time-scale events, wherein large photometric changes occur on time-scales of weeks and years. We find that the ratio of amplitudes in K_s and $W2$ can distinguish between variable accretion and variable extinction. Several YSOs are periodic or quasi-periodic variables. We identify examples of periodic accretors and extinction-driven periodicity among them (with periods up to 5 yr) though more data are needed to classify some cases. The data suggest that dynamic interactions with a companion may control the accretion rate in a substantial proportion of eruptive systems, although star–disc interactions should also be considered.

Key words: stars: AGB and post-AGB – stars: pre-main-sequence – stars: protostars – stars: variables: T Tauri, Herbig Ae/Be – stars: Wolf–Rayet – infrared: stars.

1 INTRODUCTION

Pre-main-sequence (PMS) stellar evolution is shaped by the mass accretion process (see review by Hartmann, Herczeg & Calvet 2016). As a departure from the steady mass accretion scenario (e.g. Shu 1977), episodic accretion during the PMS evolution was originally proposed to solve the luminosity problem (Kenyon et al. 1990; Hartmann & Kenyon 1996), specifically the underluminosity of low-mass Class I young stellar objects (YSOs). The mass accretion rate of a YSO would be enhanced by up to 4 orders of magnitudes

for relatively short periods (Dunham & Vorobyov 2012; Audard et al. 2014) and the luminosity would be lower at other times. Theoretical models explored several physical mechanisms that might trigger episodic accretion, including outside–in thermal instability introduced by a massive planet (Lodato & Clarke 2004; Clarke et al. 2005), imbalance between accretion controlled by gravitational and magnetorotational instabilities at different radii within the disc (Zhu, Hartmann & Gammie 2009b), disc fragmentation (Vorobyov & Basu 2005, 2010), or piling up of disc materials outside the star–disc corotation radius (D'Angelo & Spruit 2010, 2012).

Photometric variations related to episodic accretion have been observed among Class I and Class II objects with a wide range of

★ E-mail: z.guo4@herts.ac.uk

amplitudes and time-scales (see review by Audard et al. 2014, and references therein). In general, most eruptive YSOs were sorted into two groups, EXors and FUors. EXors have amplitudes up to ΔV = 5 mag (Lorenzetti et al. 2009) on time-scales of a few hundred days, and some of them have repeated outbursts (Herbig 1989, 2008; Audard et al. 2010). Spectroscopic studies revealed that EXors are undergoing the magnetospheric accretion process with indicators like broad H I recombination emission lines (e.g. Lorenzetti et al. 2009). FUors typically have similarly high amplitudes but much longer-lasting outbursts, with a rapid rise ($\sim$100 d) followed by a century-long decay (Hartmann & Kenyon 1996; Kenyon et al. 2000). Most FUor outbursts have higher luminosity than EXors with high-mass accretion rate (10^{-5} to 10^{-4} $M_\odot yr^{-1}$). The mass accretion process of FUors is not controlled by the stellar magnetic field. As a consequence, their near-infrared spectra are dominated by broad H_2O and CO absorption bands; Br γ emission is not seen and the Paschen lines are often detected in absorption (Connelley & Reipurth 2018). As the prototype of FUors, an extended self-luminous disc is found around FU Ori, as a consequence of inefficient radiative transfer throughout the geometrically thick disc (Zhu et al. 2007, 2009a; Hartmann, Zhu & Calvet 2011).

Recently, more eruptive YSOs were discovered not belonging to the EXor and FUor categories. A few YSOs show intermediate amplitude and time-scale, while having similar spectral features to FUors, e.g. HBC 722 (Kóspál et al. 2016) and V371 Ser (Hodapp et al. 2012). On the other hand, some eruptive YSOs with emission-line spectra have variation time-scales longer than typical EXors, for example, V1647 Ori (Aspin et al. 2009) and Gaia19bey (Hodapp et al. 2020). The YSO V346 Nor has unique characteristics, with an FUor-like outburst duration but an outflow-dominated spectrum (Kóspál et al. 2020). A more complete sample of eruptive objects is necessary to draw a whole picture of the episodic accretion process throughout the PMS evolution.

The VISTA Variables in the Via Lactea (VVV) survey has imaged the southern Galactic plane and the bulge in the near-infrared at several dozen epochs since 2010 (Minniti et al. 2010; Saito et al. 2012). The initial VVV survey was extended as '*VVVX*' in 2016 (Minniti 2016), so K_s (2.15 μm) light curves of 10^9 targets have been observed on a time-scale of a decade. A series of works have been carried out to study eruptive YSOs in the VVV field.[1] Contreras Peña et al. (2017a, hereafter Paper I), discovered 816 high amplitude variables from the 2010–2014 VVV K_s-band light curves ($\Delta K_s >$ 1 mag). This work showed that eruptive variability is at least an order of magnitude more common in Class I YSOs than Class II YSOs (see also Contreras Peña, Naylor & Morrell 2019). The spectroscopic follow-up work (Contreras Peña et al. 2017b, hereafter referred to as Paper II) found that most Class I eruptive variables have outbursts of intermediate duration, typically 1–5 yr, while the nature of the spectra (EXor-like emission or FUor-like absorption) in many cases did not fit expectations based on the duration of classical FUor and EXor outbursts in optically bright systems. Optically detected FUors and EXors have Class II or flat-spectrum spectral energy distributions (SEDs) suggesting a more evolved nature, though some appear to have massive circumstellar envelopes despite this (Green et al. 2013; Fehér et al. 2017). A new category of eruptive YSOs 'MNors' was tentatively proposed for these systems having intermediate outburst duration or inconsistent spectroscopic and time domain characteristics according to the classical FUor/EXor scheme.

This was a broad classification, including not only sources with 'eruptive' light curves but also some that showed evidence for long-period accretion-driven variability, dubbed 'LPV-YSOs'. Guo et al. (2020, Paper III) studied the near-infrared spectroscopic variation of 14 eruptive objects from the Paper II sample, on day-to-day and year-to-year time-scales. Both variable mass accretion and variable line-of-sight extinction were found on long-term eruptive Class I objects. In Paper III, we also defined a new type of variable YSO, the 'multiple time-scale variable' (MTV), wherein the amplitudes on short time-scales ($t < 30$ d) are comparable to the slower inter-year variations. MTVs have emission-line spectra, consistent with the magnetospheric accretion scenario. The physical mechanisms of these month-long variations are likely due to unstable accretion, but this is unclear at present.

In this work, we conducted near-infrared spectroscopic follow-up of 38 highly variable YSO candidates from the VVV survey with a variety of light-curve types. When added to the previous sample of Paper II, the combined sample size is 61 spectroscopically confirmed YSOs. Here, this large spectroscopic sample, dominated by eruptive YSOs, is used to constrain/infer the accretion mode, measure accretion luminosity, and the accretion burst duration, thereby allowing us to study the detailed nature of episodic accretion in embedded protostars. We classify the YSOs in various subtypes via their spectroscopic and multiwavelength time domain properties. The observational behaviours and underlying physical processes are then further investigated.

This paper is organized as follows: Target selection methods, observational information, and data reduction routines are described in Section 2. Spectroscopic and photometric results and target classifications are shown in Section 3. In Section 4, we discuss variation mechanisms by studying multiwavelength light curves, then take a statistical view of eruptive YSOs in the VVV survey and give details of a few individual objects. A conclusion is presented in Section 5.

2 OBSERVATION AND DATA REDUCTION

2.1 Target selection and basic information

In this paper, 38 targets were selected for follow-up in our 2017 and 2019 spectroscopic campaigns based on their variability in K_s in the VVV survey and evidence for star formation activity in the surrounding field. For the 2017 observations, 24 objects were selected from our previous study of the VVV light curves from 2010 to 2014 (Paper I), which had provided a list of 816 near-infrared variable stars with $\Delta K_s > 1$ mag. These objects were sufficiently bright ($K_s \leq 14.5$) in 2017 to allow good quality data to be obtained at intermediate resolution in brief observations. They were chosen to encompass a range of the light-curve types defined in Paper I: 'eruptive', 'dipper', 'fader', and 'LPV-YSO' (long-period variable YSO). This broadens the selection compared to the sample in Paper II, which was heavily weighted towards YSOs with eruptive light curves. Short-term variables ('denoted STV', whether periodic or not) were not selected, these almost always having $\Delta K_s \leq 1.5$ mag in Paper I. However, v618, a source previously classified as 'LPV-YSO' is reclassified as 'STV'. Herein, we use a single 'v' prefix for 21 of these 24 sources, as opposed to 'VVVv' in Paper I. The remaining three have the prefix 'Stim', denoting the discoverer W. Stimson, a previous group member in the University of Hertfordshire who identified a total of 14 highly variable stars during completeness testing in Paper I that were not included in the published list. We give details of these sources in Appendix A.

---

[1] The VVV field covers the Galactic bulge ($-10° < b < 5°$) and disc ($|b| < 2°$) with longitude $-65° < l < 10°$. *VVVX* also covers a large new area but that does not form part of this study

Table 1. Basic information for all observed targets.

Name	RA J2000	Dec. J2000	K_s (mag)	ΔK_s (mag)	$\Delta W2$ (mag)	$\Delta K_{s,WISE}$ (mag)	α_{class}	Variable star class[a]	class[b]	t_{phot}[c] (d)	Period Y/N	d_{SFR} (kpc)
v14	12:12:18.13	−62:49:04.5	15.56	1.64	0.44	1.16	0.61	LPV-YSO	M	398	Y	2.5
v16	12:13:29.76	−62:41:07.7	13.65	1.66	0.35	1.66	0.07	Eruptive	L	> 3477	N	9.7
v51	13:19:42.87	−63:01:01.9	14.56	2.93	0.60	2.71	–	AGB	L	1000	N	–
v53	13:27:02.40	−63:06:22.5	14.56	2.42	1.29	1.66	0.61	Eruptive	M	236	N	–
v84	14:09:11.55	−61:32:24.3	11.99	2.76	–	–	–	Nova	L	> 500	N	–
v128	14:58:29.67	−59:09:40.3	14.41	2.54	0.83	1.79	0.56	Eruptive	L	> 1132	N	2.6
v181	15:46:39.17	−55:50:28.3	12.76	3.47	1.58	1.41	0.58	Eruptive	M	183.9	Y?	–
v190	15:47:03.56	−54:43:10.2	13.53	1.44	0.67	0.80	− 0.43	LPV-YSO	L	612	Y	5.0
v237	16:10:48.22	−51:42:45.0	13.95	1.92	0.16	0.91	1.02	Dipper?	L	1943	N	4.2
v309	16:40:58.19	−47:06:31.9	13.56	2.60	0.28	1.17	1.30	LPV-YSO?	M	181	Y?	12.2
v319	16:45:17.04	−46:05:55.4	11.66	1.56	0.75	0.79	–	Symbiotic	L	307	Y	–
v335	16:52:09.73	−45:52:49.6	13.00	3.63	0.74	1.64	0.45	Dipper	L	1041	N	2.3
v370	16:57:48.65	−43:04:42.5	11.82	0.94	0.34	0.62	–	Symbiotic	L	419	Y	–
v371	16:59:50.04	−43:17:21.6	14.56	2.09	–	–	–	Wolf-Rayet	M	193	Y	–
v376	16:58:44.44	−42:47:36.6	12.49	1.71	0.62	0.81	− 0.37	Fader	M	>1300	N	–
v389	17:03:17.18	−42:25:49.9	13.59	1.97	0.56	1.57	0.69	Eruptive?	M	1036	N	2.2
v467	13:01:13.23	−62:25:27.9	12.79	2.64	0.85	2.37	− 0.24	LPV-YSO	L	1840	Y	4.5
v618	15:42:54.67	−55:00:52.8	12.13	1.33	0.60	0.94	− 0.09	STV	M	140	N	–
v621	15:43:12.04	−54:23:08.8	15.45	1.91	0.51	0.25	− 0.05	Eruptive	L	> 2898	N	6.0
v636	15:51:46.28	−53:25:57.3	13.60	1.43	0.62	0.96	0.43	LPV-YSO	M	565	Y	2.8
v713	16:33:52.79	−46:52:18.5	11.75	2.03	1.60	2.03	− 0.04	Fader	L	> 1130	N	3.2
Stim1	12:57:44.23	−62:15:06.4	14.20	2.45	1.70	2.45	0.63	Eruptive	L	> 3452	N	–
Stim5	16:12:14.38	−51:50:24.6	12.78	3.81	1.71	3.81	0.9	Eruptive	L	> 3452	N	2.4
Stim13	16:19:10.80	−51:03:53.0	12.39	1.51	0.20	0.76	1.39	Dipper	L	1588	N	3.1
DR4_v5	13:29:26.28	−62:23:26.5	14.11	3.96	0.31	0.81	0.95	Dipper	L	> 1230	N	–
DR4_v10	14:25:13.98	−60:20:20.0	15.67	3.56	0.79	1.57	1.86	Eruptive	L	> 3437	N	4.6
DR4_v15	15:07:11.11	−58:50:32.9	17.41	3.60	1.41	2.15	0.56	Eruptive	L	> 3456	N	4.3
DR4_v17	15:09:35.66	−57:35:22.6	13.69	3.83	1.10	2.80	0.79	LPV-YSO	L	1155	Y	4.0
DR4_v18	15:30:17.93	−55:34:55.1	13.19	4.52	2.22	4.37	0.21	Dipper	L	> 796	N	–
DR4_v20	15:44:26.03	−54:01:38.4	17.03	3.35	0.50	0.68	0.74	Eruptive	L	> 2913	N	2.5
DR4_v30	16:22:40.18	−49:06:26.4	13.68	3.88	1.37	2.14	0.36	STV or Eruptive	M	30	N	–
DR4_v34	16:29:06.99	−48:51:16.9	14.11	3.57	0.44	1.04	− 0.19	Eruptive	L	> 2904	N	3.2
DR4_v39	16:46:30.13	−46:04:39.7	13.56	4.76	1.06	2.01	0.57	Dipper	L	1445	N	3.0
DR4_v42	16:50:14.77	−44:03:30.7	15.74	3.36	1.26	2.38	1.02	Eruptive	L	> 900	N	5.1
DR4_v44	16:52:04.42	−43:33:26.0	15.98	3.57	1.04	1.46	0.83	Eruptive	L	> 2921	N	3.5
DR4_v55	17:29:02.42	−34:00:36.2	13.87	3.59	2.57	2.93	1.92	LPV-YSO	L	954	Y	3.4
DR4_v67	17:41:31.14	−31:26:12.1	14.03	5.30	1.45	3.37	1.05	Eruptive	L	2572	N	4.5
DR4_v89	17:50:50.54	−29:10:48.7	14.23	3.04	0.23	0.85	0.85	Eruptive	M	710	N	2.3

[a]Variable classification based on light curves and spectral features. YSOs are classified by categories defined in Paper I. LPV and STV stand for long-period variable and short-term variable, respectively. Uncertain classifications are marked with '?'.

[b]'M' as MTV defined in Paper III. MTVs have comparable or larger variation on short time-scales (within 1 yr) than the inter-year variation. 'L' represents objects with long-term variation.

[c]t_{phot} represents the typical time-scale of K_s-band variation. Definition in Section 2.6.

[d]$_{SFR}$: literature-based distance of star-forming regions within 5 arcmin.

The α_{class} of v621 is fit between 2 and 5 μm.

For the 2019 campaign, another 15 targets, mostly having eruptive light curves, were selected from a set of 27 YSO candidates found in a search of the VVV 4th Data Release (available at http://vsa.roe.ac.uk) for high amplitude variable stars of all types with ΔK_s > 3 mag. The 15 targets selected were those for which the available photometry indicated that they would likely be in a bright state during the 2019 spectroscopic campaign or at least an intermediate state. 14 targets have a 'DR4_v' prefix, following Lucas et al. (in preparation). One object 'Stim5' also appears in the previous selection and it was observed in both the 2017 and 2019 campaigns, providing a helpful comparison of results from the two different telescopes used.

The light-curve classifications of all 38 targets are refined using light curves drawn from the VVV/VIRAC2 catalogue, (Smith et al. 2018; Smith et al., in preparation). For YSOs, we follow

the method described in Paper I, with the addition of the MTV category (see Section 1). More information on light-curve analysis is shown in Section 2.6. Information on the targets, including coordinates, mean K_s magnitudes, variation amplitudes, light-curve classifications, and typical duration of variations are listed in Table 1.

The evolutionary stages of YSOs are classified by the slope between the near- and mid-infrared SEDs, as α_{class} defined by $d(\log F_\lambda)/d(\log\lambda)$ (Lada 1987). YSOs at early evolution stages (Classes 0 and I) have α_{class} > 0.3 while Class II objects with a thick disc have α_{class} < −0.3. In between, YSOs with −0.3 < α_{class} < 0.3 are defined as 'flat-spectrum' objects, as a transitional stage from Class I to Class II (Greene & Lada 2002; Großschedl et al. 2019). In this work, the infrared fluxes from 2 to 24 μm are drawn from public surveys including the K_s bandpass data from

the VVV/VIRAC2, IRAC *I*1 to *I*4 data from the *Spitzer*/GLIMPSE survey catalogue (Benjamin et al. 2003), MIPS24 data from the *Spitzer*/MIPSGAL survey (Carey et al. 2009; Gutermuth & Heyer 2015), and *W*1 to *W*4 bandpass data from the AllWISE data release of the *WISE* survey (Wright et al. 2010). *WISE* and *Spitzer* data are obtained via online catalogues at the NASA/IPAC Infrared Science Archive (*IRSA*).[2] In the Galactic plane, *WISE* photometry in *W*3 (12 μm) and *W*4 (22 μm) may be seriously compromised by the bright non-uniform background in star formation regions. Genuine sources detected in *W*1 and *W*2 can have spurious detections in *W*3 and *W*4 due to forced photometry at the same locations. To guard against this, visual inspection was performed on the Spitzer Enhanced Imaging Products (SEIP) images and the *unWISE* (Meisner, Lang & Schlegel 2017) images. In a few cases, where there is no mid-infrared detection in the *W*4 or MIPS 24 μm passbands, α_{class} derived from an SED fit between 2 and 12 μm.

For measurement of α_{class}, contemporaneous K_s and *WISE* photometry are strongly preferred. To complement the *WISE* photometry obtained in 2010, we only use VVV K_s data from 2010 to fit the SED slope. A comparison between K_s and *W*2 amplitudes will be discussed in Section 4.1. The measured α_{class} values for YSOs are listed in Table 1. Two objects, v84 and v621, lack archival *W*3 and *W*4 photometric detections. We visually inspected images from SEIP and ALLWISE and no source is seen at the given coordinates. From K_s to *W*2 and/or from *Spitzer* *I*1 to *I*4 bands, both objects have a steeply declining SED towards longer wavelengths, in line with Class III objects or main-sequence stars. Based on the α_{class} measurement, 73 per cent (24/33) of our targets are Class I objects, 21 per cent (7/33) are flat-spectrum objects, and 6 per cent (2/33) are disc-bearing Class II YSOs. Another five sources were classified as post-main-sequence objects based on their spectral features (see Section 3.2).

There are two facts for readers to note here. First, targets in our work lie in the Galactic mid-plane and so their α_{class} is slightly biased towards high values due to foreground extinction. Second, the variable nature of our targets may also bias the measurement of the α_{class} value. For example, an ongoing near-infrared outburst would reduce α_{class} if the energy is not efficiently reprocessed at far-infrared wavelengths. Conversely, a dimming due to extinction would cause a higher α_{class} value. Since most of the eruptive systems were in a quiescent state in 2010, the measurement of α_{class} for those objects is still a useful indicator of evolutionary stage. Similarly, the dippers (whose classification suggests an extinction event) underwent their dips after 2010. However, as we will see, the spectra are typically disc dominated and show H_2 emission lines (an indicator of Class I status; Greene & Lada 1996). This implies an earlier stage of evolution than classical EXors for example. A near-infrared colour–colour diagram is shown in Fig. 1. The *J*, *H*, and K_s magnitudes are obtained from several multiband photometric epochs from VVV/VVVX. For some eruptive systems, the *J* magnitude is only detected from the bright epoch in 2015 that is close to the spectroscopic epochs. To keep consistency, we hereby favoured the bright epochs for sources with more than one available epochs. For the sources lacking a *J*-bandpass detection, the *J* magnitude is artificially set to 20, the typical detection limit of VVV. These sources are marked by upward-pointing arrows in Fig. 1. Through comparison with the location of reddened classical T Tauri stars (Meyer, Calvet & Hillenbrand 1997), we see that most of Class I and flat-spectrum YSOs ($\alpha_{\mathrm{class}} > -0.3$) in this work have a K_s-bandpass excess.
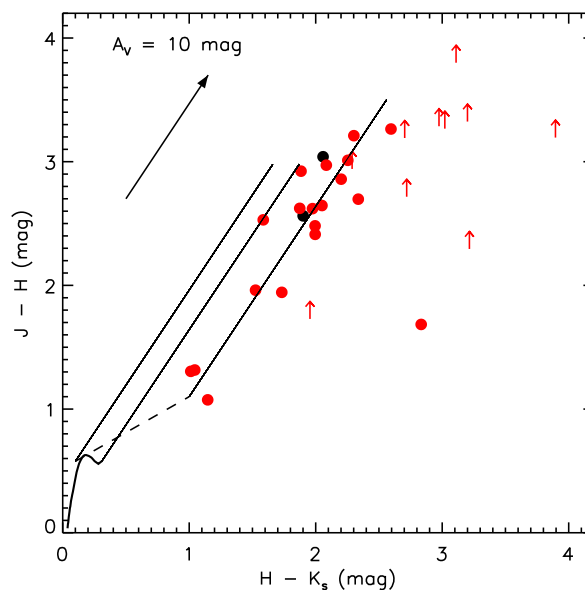
Figure 1. Colour–colour diagram for sources with *H* and *K* magnitudes in multiband epochs of the VVV/VVVX survey. Objects lack of *J* detections, marked by upward arrows, are artificially set *J* as 20 mag. Class I and flat-spectrum objects identified by α_{class} are shown by the red dots. Dashed line is the intrinsic locus of Classical T Tauri Stars (CTTS, or Class II objects) from Meyer et al. (1997). The solid curve represents the empirical colour of main-sequence stars (Pecaut & Mamajek 2013). The solid straight lines are reddening vectors assuming $R_V = 3.1$ (Wang & Chen 2019).

2.2 Spectroscopic observations

In the 2017 campaign, spectra of 24 targets were obtained using the Echelle mode of Folded-port Infra-Red Echellette (FIRE) spectrograph (Simcoe et al. 2013) on the Magellan Telescope over two consecutive nights (May 29th and 30th) at Las Campanas Observatory, Chile. The FIRE spectrograph covers the near-infrared waveband from 0.8 μm to 2.45 μm. A slit width of either 0.6 or 0.75 arcsec was used, depending on the seeing conditions, giving resolution $R \sim 6000$ or $R \sim 4500$, respectively. The data reduction procedures are similar to those described in Paper III using the FIREHOSE V2.0 pipeline (Gagne et al. 2015) plus customized programs based on the IDL platform.

The 2019 spectroscopic campaign was conducted using the slit mode of the X-shooter spectrograph (Vernet et al. 2011) on the ESO Very Large Telescope (VLT), at Paranal Observatory, Chile. Data were taken in Service Mode (program ID 0103.C-0622(A)). Both the visible and near-infrared arms were used simultaneously during the observations and the exposure time is adjusted for individual target based on the expected brightness. In this work, we only present the near-infrared spectra since a visible spectrum was detected in only one source (DR4_v30). A slit width of 0.6 arcsec was used for all targets, giving resolution $R \approx 8000$ in the K_s bandpass. Blind offsetting was applied for both spectrographs for most targets since they were typically fainter than the 20th magnitude in the acquisition images, taken in the *J* bandpass for FIRE and the *z* bandpass for X-shooter. Observation date, exposure time, and spectrograph information for individual targets are listed in Table B3.

2.3 Reduction of X-shooter spectra

Spectra were extracted by the X-shooter pipeline as constructed in the ESO Recipe Flexible Execution Workbench software (REFLEX;

Freudling et al. 2013). The data reduction workflow first creates master calibration frames, including bias, flat, and dark fields. Then the location of the spectra (taken at two separate nod positions) and the wavelength solution are generated by a 2D mapping algorithm using arc lamp frames. Sky backgrounds are extracted under the STARE reduction mode of the pipeline, which provides an additional step of wavelength calibration for individual targets. We noticed a constant 83 km s^{-1} shift between the wavelength solution provided by the pipeline and the wavelengths of the OH sky lines between 2.1 and 2.5 μm. This shift was manually corrected during the data reduction. The flux calibration was derived from telluric standard stars observed on the same night as the scientific targets. Telluric absorption lines are further corrected by the MOLECFIT software (Kausch et al. 2015; Smette et al. 2015).

An accurate absolute flux calibration could not be performed because most targets were acquired by blind offsetting and because observation of these relatively bright infrared stars was queued for relatively poor seeing conditions by Paranal standards (typically 1.0–1.5 arcsec seeing at the zenith). We present the pipeline produced fluxes for the X-shooter spectra none the less. The synthesized flux of Xshooter targets through the K_s filter is shown by a blue dot in the relevant panels in Fig. B2. The reader should be aware that the integrated flux may be less than the real flux due to imperfect target acquisition on the slit and changeable observing conditions. Examples of reduced spectra are presented in Fig. H1.

2.4 Spectroscopic measurements and CO model

Three principal spectroscopic features are measured in this work: the CO overtone bands beyond 2.29 μm, molecular hydrogen (H$_2$) emission lines, and the Br γ line at 2.166 μm. Heliocentric velocities and the sun's motion relative to the Local Standard of Rest is calculated by the data reduction pipelines and are corrected before measuring spectral features. All measurements are conducted by custom-written programs in the IDL platform. The measurements of line features followed the Gaussian fitting method developed in Paper III, and the results are shown in Table 2. The typical uncertainty of the radial velocity measurement is about 1 pixel on the array detector, which corresponds to ∼12 km s^{-1} for both detectors. In individual sources, H$_2$ emission, originating from the stellar wind or outflow, often has a blueshifted radial velocity relative to the Br γ and CO emission that trace the mass accretion process and the rotating disc. The radial velocity difference between H$_2$ and Br γ lines reaches 100 km s^{-1} in a few sources.

The ^{12}CO overtone features are measured by fitting synthetic models to the continuum-subtracted spectra. The CO model used in this work is based on previous works (Kraus et al. 2000, and appendix E in Paper II). By considering the rovibrational energy states of the CO molecule (Dunham 1932; Farrenq et al. 1991), this model calculates the spectral intensity of CO band heads for a range of temperatures and column densities. In addition, the line-of-sight Keplerian rotation velocity are now added to the previous model, for a range of disc inclination angles. The CO models are then applied to fit the first two bands ($v = 2 - 0$ and $v = 3 - 1$). As mentioned in Paper II, observed CO profiles usually have broader band heads than the models, and high Keplerian velocity from an accretion disc was proposed as an explanation of the broadened emission profile (Najita, Carr & Tokunaga 1996; Davies et al. 2010). In this work, we noticed that the unexpected broadening of the CO emission is only seen on the first ($v = 2 - 0$) band for most YSOs, while the second band ($v = 3 - 1$) is usually well fit by the model. This broadening issue could not be fully solved by adding a more realistic

disc model including the temperature gradient in the inner disc (e.g. Wheelwright et al. 2010; Ilee et al. 2013). We believe that there are some missing spectral features in the first band in our model. Hence, in our analysis and discussion we use the CO model fitting only for radial velocity measurements (which are reliable because there are many well-fitted lines in the CO bands) and we do not quote the fitted temperatures and column densities.

2.5 Distance measurements

Wherever possible, kinematic distances, d_k, were derived from the radial velocities measured in the CO overtone band fits described above. For objects without CO features, we used the radial velocity of the Br γ line to derive the kinematic distance because H$_2$ lines more often arise in a blueshifted wind or outflow. The uncertainty of the radial velocity measurement is approximately 1 array pixel, about 12 km s^{-1} in both spectrographs. The kinematic distances are measured via the 'Monte Carlo simulation mode' of the online tool provided by Wenger et al. (2018), which includes the uncertainties in the Galactic rotation model. The constants in the calculations are adopted from Reid et al. (2014), including the circular rotation speed of the Solar system ($\Theta_0 = 240 \pm 8$ km s^{-1}), the distance to the Galactic Centre ($R_0 = 8.34 \pm 0.16$ kpc), and the Galactic rotation curve. The kinematic distances and uncertainties are listed in Table 2. For targets lacking Br γ and CO features and targets for which the measured radial velocity is inconsistent with the Galactic rotation model (e.g. halo stars) distances are not given in Table 2. In addition, we noticed that the difference between the radial velocities of Br γ line and CO bandhead emission sometimes significantly exceeds the uncertainty (12 km s^{-1}). Therefore, the kinematic distance derived by the radial velocity of Br γ line alone is highly uncertain and needs to be confirmed by other methods, such as a literature-based distance to the surrounding star formation region, $d_{\rm SFR}$.

Most of our targets are heavily embedded distant Class I YSOs, very faint in the optical waveband, so *Gaia* measurements are not available. Here, the measured proper motions (PMs) of individual objects are provided in the VIRAC2[3] catalogue, which were used to break the ambiguity between the near and far kinematic distance solutions. The PM-based probability density function for distance is calculated by a Monte Carlo method built on the PYTHON platform, using one of two models of the Milky Way disc rotation and the peculiar velocity dispersion, adopted for YSOs and non-YSOs treated as Galactic 'thin disc' stars, respectively (the latter drawing on Bensby et al. 2013). For a given PM measurement, a distance solution is computed by randomly sampling from the peculiar velocity distribution and the PM error distribution using Gaussian errors.[4] The probability histogram is then generated by binning 1 million samples for each star. Kinematic distances consistent with the sometimes rather wide range of distances allowed by the PM-based distance solutions are marked by the ⋆ symbol in Table 2. Several targets lack consistent d_k and PM distance solutions, which could

---

[3]The VIRAC2 PMs, though calibrated using the *Gaia* second data release, are preliminary. The final absolute calibration, based on the *Gaia* 'eDR3' reference frame, is still in progress but any changes are expected to be very small.

[4]The approach is an evolution of that of Smith et al. (2018). Details of the adopted rotation curves and peculiar velocity distributions used for YSOs and thin disc stars in the sample will be given in a separate paper (Morris et al., in preparation). A relatively broad peculiar velocity spread (20 km s^{-1} in the U and V components) is used for YSOs in order to allow for uncertainties in the rotation curve, i.e. folding the two effects into a single parameter.

Table 2. Spectral characteristics of Br γ line, H$_2$ (2.12 µm) line, and CO band heads feature.

Object	Instrument	Br γ		H$_2$ (2.12 µm)		CO		d_k	
		RV (km s^{-1})	EW (Å)	RV (km s^{-1})	EW (Å)	RV (km s^{-1})	EW (Å)	d_{near} (kpc)	d_{far} (kpc)
Young stellar objects:									
v14	FIRE	-34.1	-5.8 ± 1.1	–	–	–	–	$\star 1.88^{+1.08}_{-0.87}$	$6.09^{+0.93}_{-1.13}$
v16	FIRE	6.3	0.4 ± 0.2	–	–	2.2	12.5 ± 7.0	–	$\star 8.20^{+1.20}_{-1.11}$
v53	FIRE	93.9	-3.6 ± 0.5	–	–	51.5	-42.6 ± 5.6	–	$\star 13.90^{+1.74}_{-1.24}$
v128	FIRE	61.3	-1.2 ± 1.0	-45.2	-0.9 ± 0.2	–	–	–	–
v181	FIRE	5.0	-4.4 ± 0.8	-48.4	-2.0 ± 0.8	18.1	-32.1 ± 8.7	–	$15.03^{+1.44}_{-1.08}$
v190	FIRE	-46.0	-2.1 ± 0.9	-135.2	-2.8 ± 0.4	-66.8	-10.3 ± 6.1	$\star 3.95^{+0.42}_{-0.38}$	$10.01^{+0.35}_{-0.57}$
v237	FIRE	-1.3	-0.5 ± 0.3	–	–	-85.1	7.8 ± 7.4	$4.96^{+0.74}_{-0.83}$	$\star 9.69^{+0.82}_{-0.82}$
v309	FIRE	-47.2	-1.7 ± 0.8	-135.3	-8.5 ± 0.4	-35.3	-31.7 ± 5.1	$\star 2.83^{+0.67}_{-0.92}$	$12.66^{+0.94}_{-0.78}$
v335	FIRE	-54.8	-4.7 ± 0.3	-41.9	-0.4 ± 0.2	-60.0	-13.0 ± 5.2	$\star 4.23^{+0.73}_{-0.79}$	$11.32^{+0.90}_{-0.60}$
v376	FIRE	-11.3	-0.9 ± 0.3	–	–	–	–	$\star 1.24^{+0.99}_{-0.85}$	$14.67^{+1.26}_{-1.26}$
v389	FIRE	-52.4	-3.4 ± 0.9	-51.2	-3.9 ± 0.3	–	–	$4.28^{+0.73}_{-0.80}$	$11.83^{+0.78}_{-0.78}$
v467	FIRE	-12.7	-0.5 ± 0.4	-66.5	-1.7 ± 0.2	-3.6	-9.9 ± 5.7	$0.20^{+0.94}_{-0.19}$	$\star 8.98^{+1.28}_{-0.85}$
v618	FIRE	–	–	-38.3	-6.0 ± 1.5	–	–	–	–
v621	FIRE	13.4	-7.1 ± 0.9	–	–	–	–	–	$14.74^{+1.44}_{-1.00}$
v636	FIRE	–	–	-43.6	-3.3 ± 0.3	–	–	–	–
v713	FIRE	-76.4	-3.4 ± 0.7	-47.3	-2.8 ± 0.2	-49.5	-15.3 ± 13.6	$\star 3.51^{+0.68}_{-0.81}$	$11.87^{+0.89}_{-0.67}$
Stim1	FIRE	-2.0	-3.3 ± 0.3	–	–	17.8	-18.7 ± 3.1	–	$10.50^{+1.14}_{-1.06}$
Stim5	FIRE	-97.1	-2.9 ± 0.7	-127.5	-2.2 ± 0.4	-91.2	-34.0 ± 5.2	$\star 5.14^{+0.83}_{-0.73}$	$9.52^{+0.72}_{-0.92}$
Stim5	XSHOOTER	-91.5	-2.6 ± 2.0	-159.2	-14.2 ± 0.1	-78.7	-22.1 ± 14.2	$\star 4.49^{+0.88}_{-0.66}$	$10.15^{+0.71}_{-0.93}$
Stim13	FIRE	-40.1	-1.3 ± 0.9	-51.0	-2.9 ± 0.5	–	–	$\star 2.68^{+0.75}_{-0.75}$	$12.04^{+0.86}_{-0.73}$
DR4_v5	XSHOOTER	–	–	-79.0	-9.1 ± 0.5	-27.9	-25.8 ± 12.2	$\star 1.82^{+1.12}_{-0.96}$	$8.26^{+1.03}_{-1.17}$
DR4_v10	XSHOOTER	-105.3	-4.0 ± 0.8	-84.4	-1.7 ± 0.3	-78.2	-8.9 ± 6.1	$\star 4.25^{+1.01}_{-0.54}$	$\star 7.30^{+0.62}_{-0.91}$
DR4_v15	XSHOOTER	–	–	-90.5	-3.1 ± 0.1	–	–	–	–
DR4_v17	XSHOOTER	-98.1	-1.2 ± 0.4	-126.3	-2.1 ± 0.4	-73.1	-12.2 ± 6.5	$\star 4.34^{+0.89}_{-0.84}$	$8.62^{+0.78}_{-0.95}$
DR4_v18	XSHOOTER	-100.0	-3.0 ± 0.4	-83.8	-1.0 ± 0.2	-90.2	-6.9 ± 5.7	$\star 5.18^{+0.74}_{-0.82}$	$8.25^{+0.89}_{-0.67}$
DR4_v20	XSHOOTER	–	–	-48.4	-2.5 ± 0.5	-83.7	40.6 ± 9.2	$\star 4.67^{+0.97}_{-0.67}$	$9.26^{+0.69}_{-0.98}$
DR4_v30	XSHOOTER	-143.3	-1.1 ± 0.1	–	–	-126.8	-1.9 ± 0.6	$\star 6.65^{+0.39}_{-0.78}$	$8.35^{+0.86}_{-0.38}$
DR4_v34	XSHOOTER	-58.4	-3.8 ± 0.2	-121.0	-3.8 ± 0.3	-59.4	-28.4 ± 3.5	$\star 3.95^{+0.54}_{-0.90}$	$11.21^{+0.90}_{-0.60}$
DR4_v39	XSHOOTER	–	–	-77.3	-35.3 ± 0.9	-72.5	-7.5 ± 16.0	$\star 4.63^{+0.81}_{-0.64}$	$10.98^{+0.64}_{-0.87}$
DR4_v42	XSHOOTER	-111.0	-4.8 ± 0.9	-117.9	-23.3 ± 0.2	-114.7	-17.4 ± 17.6	$6.56^{+0.66}_{-0.62}$	$9.21^{+0.65}_{-0.65}$
DR4_v44	XSHOOTER	-85.0	-2.1 ± 0.3	–	–	-48.9	-25.4 ± 6.3	$\star 3.87^{+0.73}_{-0.81}$	$11.98^{+0.93}_{-0.77}$
DR4_v55	XSHOOTER	–	–	-34.7	-30.5 ± 1.3	–	–	–	–
DR4_v67	XSHOOTER	–	–	-43.4	-12.1 ± 0.1	–	–	–	–
DR4_v89	XSHOOTER	–	–	-51.4	-5.2 ± 0.3	–	–	–	–
Post-main-sequence objects:									
v51	FIRE	-34.3	0.9 ± 0.5	–	–	37.3	7.8 ± 5.6	–	$\star 12.46^{+1.48}_{-1.06}$
v84	FIRE	$-218.9; 208.0$	-5.8 ± 0.7	–	–	–	–	–	–
v319	FIRE	128.6	1.1 ± 0.4	–	–	119.8	56.9 ± 6.1	–	–
v370	FIRE	26.1	-0.9 ± 0.4	–	–	-10.2	49.9 ± 10.8	$\star 1.45^{+0.74}_{-1.07}$	$\star 14.61^{+1.41}_{-1.16}$
v371	FIRE	-88.2	-30.7 ± 3.7	–	–	–	–	$5.79^{+0.72}_{-0.72}$	$10.21^{+0.66}_{-0.76}$

Notes. The spectral resolutions of the FIRE and XSHOOTER spectra are about 50 and 37 km s^{-1}, respectively. The uncertainty of the radial velocity measurement is equivalent to the pixel size of the array detector, which is about 12 km s^{-1} in both spectrographs.
$\star$: Kinematic distances agree with PM distance solutions.

be due to underestimated errors in the PM measurements for faint objects, large orbital motions in binary systems, intrinsic blueshifts of expanding CO shells around asymptotic giant branch (AGB) stars, or a Galactic halo location.

2.6 Light-curve analysis

The 2010–2015 K_s light curves of 21 targets with the 'v' prefix were previously published in Paper I, based on aperture photometry. In this work, we present a new set of VVV/VIRAC2 K_s light curves

for all 61 targets in the combined sample (see online supplementary information, examples are shown in Table B1). The light curves, contain K_s profile fitting photometry from 2010 to 2019. The profile fitting photometry was carried out with DOPHOT (Schechter, Mateo & Saha 1993; Alonso-García et al. 2012). The absolute photometric calibration of the VIRAC2 catalogue is based on a new procedure designed to mitigate issues pointed out by Hajdu et al. (2020) that arise from blending of multiple VVV sources in 2MASS data for very crowded star fields in the inner Galactic bulge.

We applied the χ-value, an output of DOPHOT, from the VIRAC2 catalogue as a selection criteria in order to remove less reliable data points. Detections with χ-value >3 are excluded from the final light curves. As a second step, the relation between K_s magnitudes and photometric errors (δK_s) is fitted by a third-order polynomial function derived from all sources in this work. All sources share the same K_s versus δK_s relationship. Detections with δK_s deviating from this relationship by more than 3σ are rejected from the final light curves. The typical photometric error is 0.020 mag at $K_s = 11$ mag and 0.069 mag at $K_s = 16$ mag. In the final light curves (shown in Figs B1 and B2), the data are averaged in 1 d bins because this work focuses on longer term variability rather than intranight changes. Even though the error reported by DOPHOT is small, the magnitudes above $K_s = 11.25$ mag, could suffer from a not so completely linear response from the detector.

The photometric period of individual object is measured using the generalized Lomb–Scargle periodogram in IDL (Zechmeister & Kürster 2009). More details are shown in Section 3.3. The variation time-scale (t_{phot}) is defined as follows. For periodic variables, t_{phot} is the photometric period (see Table 1). For other YSOs, t_{phot} is the time difference between two photometric minima for sources with eruptive light curves and the time between maxima for 'dippers'. For objects with ongoing outbursts and decays, we indicate in Table 1 that t_{phot} is a lower limit. The nature of photometric variations is summarized in Table 1.

3 RESULTS

In this section, we will present the spectral features of our targets, period analysis, and classifications of variables based on both spectroscopic and photometric information.

3.1 Spectroscopic features of accretion modes of YSOs

The spectroscopic features of YSOs are shaped by mass accretion process (Hartmann & Kenyon 1996; Hartmann et al. 2016). In general, there are two types of accretion natures in YSOs that are distinguishable by certain spectral features. Magnetospheric accretion and boundary layer accretion were introduced in section 3.1 of Paper III and references therein. Here, we briefly summarize the spectral features of these two accretion scenarios.

Magnetospheric accretion is widely observed on disc-bearing YSOs. Emission features are generated around the accretion shock on the stellar surface, such as H I recombination lines (e.g. Pa β and Br γ) and Ca II triplet (8498, 8542, and 8662 Å). Emission fluxes of Ca II and H I recombination lines have tight empirical correlations with the mass accretion rate (Muzerolle, Hartmann & Calvet 1998; Alcalá et al. 2014). Originating from the chromosphere and the disc, the Na I emission doublet at 2.206 μm is closely correlated with Br γ emission (Paper III). Recent near-infrared surveys found CO overtone emission bands, although excited in the inner gaseous disc, have a positive correlation with Br γ emission on both non-eruptive (Connelley & Greene 2010) and eruptive YSOs (Kóspál et al. 2011b; Paper III), indicating that CO emission is associated with a high rate of magnetospheric accretion, perhaps due to irradiation by hotspots on the star arising from the accretion columns (Hodapp et al. 2020).

Boundary layer accretion, mostly seen in FUors, shows strong H_2O and CO absorption bands arising in cool upper layers of its self-luminous accretion disc (see review by Audard et al. 2014). In Paper III, we found stronger CO absorption is associated with a brighter near-infrared continuum that is consistent with the physical expectation that the disc's vertical temperature gradient is steeper

when the accretion rate is higher and more energy is being released in the disc's mid-plane. Weak photospheric CO absorption features are seen in YSOs and they are associated with other absorption lines (e.g. Na I and Ca I) (Johns-Krull & Valenti 2001; Paper II). In addition, strong CO absorption is also observed in the photosphere of very low mass YSOs (e.g. Lucas et al. 2001; Allers et al. 2007; Jose et al. 2020), which are much less luminous than FUor outbursts and hence should be much less distant. Leaving aside these cases of photospheric absorption, the strong CO overtone absorption in a distant eruptive YSO is an efficient indicator of boundary layer accretion process. For the following results and discussions, YSOs are termed 'FUor-like' when CO absorption features are detected.

The near-infrared H_2 emission lines are indicators of stellar winds and outflows (Chrysostomou et al. 2008; Greene, Barsony & Weintraub 2010). Although seen in non-variable sources like protoplanetary nebulae, H_2 lines are recognized as signatures of YSOs. After inspecting samples of eruptive YSO spectra (Connelley & Reipurth 2018; Paper III), we found the strength of H_2 emission lines is independent of variation in other spectral features. The absence of H_2 emission in most FUors might be a veiling effect of the hot self-luminous disc (see discussions of v332 in section 4.2.3 of Paper III) or rather the absence of collimated winds/jets during the FUor burst.

3.2 Spectroscopic classification

Here, we identify non-YSOs in the sample and then sort the variable YSOs into two categories based on their spectral features. YSOs with ^{12}CO ($\Delta \nu = 2$) overtone absorption beyond 2.29 μm are classified as 'FUor-like' objects, and YSOs with emission features (e.g. H_2, Br γ, Na I, or CO emission) are classified as 'emission-line spectra' YSOs. The spectral characteristics of our targets are summarized in Table 3.

3.2.1 Emission-line YSOs

33 of the 38 new spectroscopic targets observed in this work are identified as YSOs. Br γ emission is clearly detected in 23 of them and there is a marginal detection ($\sim$1.5σ) in one additional source, v237. Other indicators of magnetospheric accretion, including Pa β emission, Na I emission, and CO overtone emission, are only observed among objects with Br γ emission, with the exception of DR4_v39. H_2 emission lines are seen in 24 YSOs. Following the classification methods introduced above, there are 30 YSOs classified as 'emission-line objects'. This category includes 24 YSOs with indicators of magnetospheric accretion and five YSOs with 'outflow-dominated' spectra, these displaying only H_2 emission, sometimes accompanied by [Fe II] emission. One object (v621) has debatable spectral features as broad Br γ and He I emission lines, which are often observed on nova. However, the light curve of v621 had a quick rise and then stayed on a brightness plateau for at least 6.5 yr, which has not seen among novae. Hence, we still classify v621 as an eruptive YSO.

3.2.2 FUor-like YSOs

CO overtone absorption is observed in six of the new spectroscopic targets, three of which are identified as FUor-like YSOs. Two of the three YSOs also display water vapour absorption bands. When we include FUor-like VVV sources from Paper II, there are six YSOs with FUor-like spectra in the combined sample. These are v16, v237, DR4_v20, v322, v721, and v717. Of the three new FUor-like YSOs listed in Table 3, one (v237) has marginally detected Br γ emission, as

Table 3. Spectral characteristics and classifications.

Name	Br γ	Pa β	Na I	H$_2^a$	CO	H$_2$O	Spec. class
H$_2$ emission only							
Outflow dominated							
v618	–	–	–	E	–	–	Emission line
DR4_v15	–	–	–	E	–	–	Emission line
DR4_v55	–	–	–	E	–	–	Emission line
DR4_v67	–	–	–	E	–	–	Emission line
DR4_v89	–	–	–	E	–	–	Emission line
H$_2$, Br γ, and/or CO bandhead emission							
v14	E	–	–	–	–	–	Emission line
v53	E	–	E	–	E		Emission line
v128	E	–	–	E	–	A	Emission line
v181	E	E	–	E	E	–	Emission line
v190	E	–	E	E	E	–	Emission line
v309	E	–	E	E	E	–	Emission line
v335	E	E	E	E	E	–	Emission line
v376	E	–	–	–	–	–	Emission line
v389	E	–	–	E	–	–	Emission line
v467	E	–	–	E	E	–	Emission line
v621	E	–	–	–	?	–	Emission line
v636	E?	–	–	E	–	–	Emission line
v713	E	E	–	E	–	–	Emission line
Stim1	E	E	E	–	E	–	Emission line
Stim13	E	–	–	E	–	–	Emission line
Stim5	E	–	E	E	E	–	Emission line
DR4_v5	E	–	–	E	E	–	Emission line
DR4_v10	E	–	–	E	E	–	Emission line
DR4_v17	E	–	–	E	E	–	Emission line
DR4_v18	E	E	E	E	E	–	Emission line
DR4_v30	E	E	–	–	E	–	Emission line
DR4_v34	E	E	E	E	E	–	Emission line
DR4_v39	–	–	–	E	E	–	Emission line
DR4_v42	E	–	–	E	E	–	Emission line
DR4_v44	E	E	E	–	E	–	Emission line
CO absorption							
v16	A	–	–	–	A	A	FUor-like
v237	E	–	–	–	A	–	FUor-like
DR4_v20	–	–	–	E	A	A	FUor-like
Post-main-sequence objects							
v51	–	–	–	–	A	A	AGB
v319	E	–	–	–	A	–	Symbiotic
v370	E	–	–	–	A	A	Symbiotic
v84	E	–	E	E	–	–	Nova
v371	E	–	–	–	–	–	Wolf–Rayet

Notes. Emission lines or band features are marked by 'E' while absorption features are marked by 'A'. Non-detections are shown by '–'.
^{a}H$_2$ 1–0 S(1) line at 2.12 μm.
In Section 4.2, YSOs only have H$_2$ emission in their spectra and are classified as 'outflow dominated' sources.

noted above, one (v16) has marginally detected Br γ absorption, and one (DR4_v20) has no Br γ detection but displays clear H$_2$ emission lines. Due to the large photometric variability of the three and their large distances (see Table 1), there is no possibility of confusion between FUor-like YSOs and very young brown dwarfs having CO and water vapour absorption in the photosphere.

3.2.3 Non-YSOs

Among the six new spectroscopic targets displaying ^{12}CO overtone absorption, three also show the ^{12}CO second overtone ($\Delta\nu = 3$) absorption bands in the *H* bandpass and/or strong ^{13}CO ($\nu = 2 - 0$)

first overtone absorption. These three are then identified as AGB stars (v51, v319, and v370, Section G). In the case of v51, since there were only two dips in the light curve, it may have a 2500 d period. However, the brightness is very different before and after the first dip so it may be aperiodic. The other two AGB stars have periods of a few hundred days, which are typical for Mira variables.

In addition, double-peaked and broad Br γ emission associated with He I or He II emission lines are detected in two sources. The spectrum of v371 is very similar to that of a Wolf–Rayet type star, with strong He II emission lines blended with Br γ emission and broad N III emission at 2.11 μm (Mauerhan, Van Dyk & Morris 2009). We name v371 as WR80-1 following the up-to-date naming convention of massive stars (Rosslowe & Crowther 2015).[5] A 193 d quasi-period is found in the VVV light curve of this star. Although periodic variation is widely detected in Wolf–Rayet type stars, the 193 d period is longer than the time-scale of wind-dominated variation (WR 1, 16.9 d; Chené & St-Louis 2010) and is much shorter than the multiyear-long dust making process (Williams 2019). We therefore suggest that v371 is perhaps in a binary system.

V84 has a blue SED ($\alpha = -2.3$) and the light curve shows a fading trend with $\Delta K_s = 2.76$ mag in the first 600 d of the VVV survey. It remained at a low brightness level thereafter. Strong double-peaked He I and Br γ emission lines are detected, suggesting a fast rotating envelope ($v \sim 200$ km s^{-1}). Both photometric and spectroscopic features of v84 are consistent with previously detected novae, such as v514 in Paper II, V1493 Aql (Venturini et al. 2004), and V2491 Cyg (Naik, Banerjee & Ashok 2009). Towards the end of the VVV VIRAC2 light curve, the brightness of v84 shows signs of rising again slightly. It might therefore be a recurrent nova, though significant photometric variations are also seen in classical novae long after the outburst.

3.2.4 The combined sample

Including sources from Paper II, 75 high-amplitude VVV variable stars have near-infrared spectra. Following the spectroscopic classification above, 61 sources are confirmed as YSOs: 6 FUor-like objects and 55 emission-line objects. Of the 55 emission-line objects, 46 YSOs have signatures of magnetospheric accretion, including 45 having H I recombination line emission and one source (DR4_v39) lacking this feature but having CO overtone emission. The remaining eight emission-line YSOs have outflow-dominated spectra so their accretion modes are not yet determined. According to the spectral indices calculated in Section 2.1 and Paper II, about 2/3 of these spectroscopically confirmed YSOs are Class I objects (40/61), some of them are flat-spectrum objects (17/61), and 4 of them are Class II objects.

3.3 Periodic or quasi-periodic variables

Most periodic variations on YSOs are associated with stellar or disc rotation. For instance, star-spots on Class II/III objects have sinusoidal variation on time-scales from days to weeks (e.g. Guo, Gully-Santiago & Herczeg 2018b; Rebull et al. 2018). Periodic extinction by asymmetric inner disc structures is mostly seen on Class II objects on time-scales from one week to months (e.g. Bouvier et al. 2007). Although most episodic accretion bursts (FUor- and EXor-type) are unpredictable in Class 0/I objects, three YSOs in the literature display periodic variability attributed to a large and
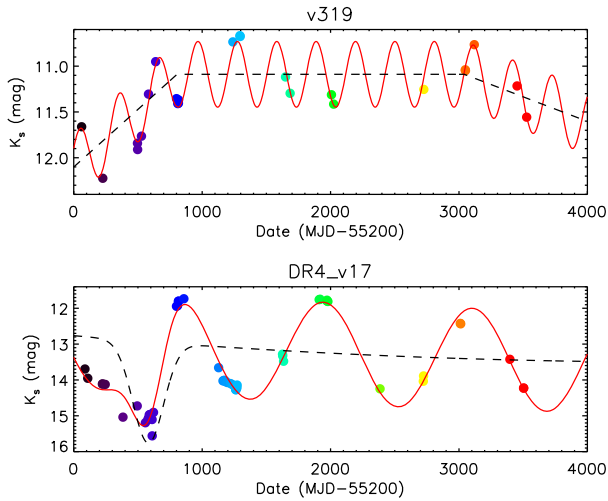
[5] http://pacrowther.staff.shef.ac.uk/WRcat

Figure 2. The K_s-band VVV light curve of v319 and DR4_v17. Data points are colour coded by the observation time. The long-term trends are fitted by the dashed lines, and the overall variations are fitted red solid lines.

periodic change in the accretion rate. Periodic accretion events seen in the Class I YSOs LRLL 54361 (25 d, Muzerolle et al. 2013) and V347 Aur (160 d, Dahm & Hillenbrand 2020) are presumably triggered by undetected stellar companions. A ∼530 d periodic accretion flare is observed on the Class 0 object EC53 (V371 Ser) by both near-infrared and millimetre surveys (Hodapp et al. 2012; Lee et al. 2020), which is interpreted as a consequence of piled-up material in the inner disc.

Periodic VVV variables were identified in Paper I from 2010 to 2015 light curves by phase dispersion minimization (PDM) method. In this work, we applied generalized Lomb–Scargle periodogram (Zechmeister & Kürster 2009) to VIRAC2 version light curves of spectroscopic followed up variables in this work and spectroscopic confirmed YSOs from Paper II. Light-curve data are averaged in 1 d bins to avoid the oversampling issue. The fitting period is constrained to be in the range of 10–2000 d, based on the cadence of the light curves and the duration of the VVV survey. The best-fitting period is identified by the highest peak in the periodogram. Two particular targets, v319 and DR4_v17 have light curves that are combinations of long-term ($t > 500$ d) trends and periodic variations. Hence, their power spectra were generated after fitting and removing the long-term trends (see Fig. 2). Finally, we visually inspected the phase-folded light curves to confirm the periods.

In total, 16 objects have periods in their light curves ranging from 30 to 1840 d. All measured periods passed the 1 per cent false alarm possibility test (method from Guo et al. 2018a). The residual to the fit in the phase-folded light curves is used to categorize these objects as periodic or quasi-periodic. The phase-folded light curves are fitted with the following analytical functions (for the purpose of this categorization only): Gaussian, polynomial burst, and sinusoidal curves, examples of which are given in Fig. B3. Objects are defined as periodic if the standard deviation of the fitting residual is smaller than 10 per cent of the amplitude in K_s. Under this definition, five objects are identified as periodic variables and 11 objects as quasi-periodic variables (listed in Table 4). The longest period is seen on v467 ($P = 1840$ d), which shows two dips in the unfolded light curve. The periodicity of this source is yet to be confirmed as only two full periods were observed within the VVV survey.

Two quasi-periodic variables have periods around 180 d, which are suspicious as they might be false periods introduced by the

Table 4. Periodic variables from VVV light curves.

Name	Period (d) this work	Period (d) Paper I	ΔK_s (mag)	δ_{K_s} (mag)	Class
YSOs from this work:					
v14	397	124	1.64	0.21	Q
v190	611	125	1.44	0.22	Q
v467[a]	1840	–	2.64	0.24	P
v636	565	609	1.43	0.21	Q
DR4_v17	1154	–	3.03	0.12	P
DR4_v55	953	–	3.59	0.34	P
v181[b]	184	–	3.49	0.55	Q
v309[b]	181	191	2.60	0.43	Q
YSOs from Paper II:					
v32	1439	–	1.80	0.18	P
v65	30.2	30	0.98	0.21	Q
v94	436	–	1.27	0.24	Q
v480	306	303	1.51	0.24	Q
v630	409	–	1.57	0.31	Q
Post-main-sequence objects:					
v319	307	–	0.86	0.07	P
v370	419	445	0.94	0.11	Q
v371	193	186	2.09	0.28	Q

Notes. δ_{K_s}: Fitting residual on the phase-folded light curve.
Class: Periodic (P) or quasi-periodic (Q) variable.
[a]Only two full periods were detected in the VVV light curve.
[b]Sources with suspicious half-year periods and doubtful periodicity.

observational cadence (i.e. one to three epochs close together in each year from 2016 to 2019). Both of them have large fitting residuals ($\delta K_s > 0.4$ mag). In particular, the unfolded light curve of v181 is a combination of a sharp dip ($t \sim 100$ d) and a gradual long-term variation. It is possible that the observed light-curve features arise from a poorly sampled periodic variation, but the evidence is fairly weak. In this case, the 184 d period on v181 is highly doubtful so we list it as 'eruptive' rather than 'LPV-YSO' in Table 1.

Eight YSOs have periods detected by the PDM method in Paper I, including six with similar periods in the two works. Two objects have longer periods measured in this work than the results from Paper I. The period of v14 measured in Paper I corresponds to the second highest peak in the periodogram generated in this work. Among the other eight objects without periods in Paper I, DR4_v17 and DR4_v55 are new sources first studied in this work, v32 and v467 have periods longer than 1000 d, and the rest were classified as aperiodic in Paper I.

Based on the spectroscopic features, 13 periodic or quasi-periodic variables are identified as YSOs, and all of them are emission-line YSOs. In the following section, we will discuss the near-to-mid-infrared amplitude of long-term periodic YSOs (v32, DR4_v17, and DR4_v55), in order to identify periodic accretion bursts. Separately, one periodic and two quasi-periodic objects are identified as post-main-sequence stars: two AGB stars (see Section G) and a Wolf–Rayet star.

4 DISCUSSION

4.1 Near-infrared colour variation

The variation mechanisms of eruptive objects can be revealed by infrared colour changes. For example, the optical to near-infrared
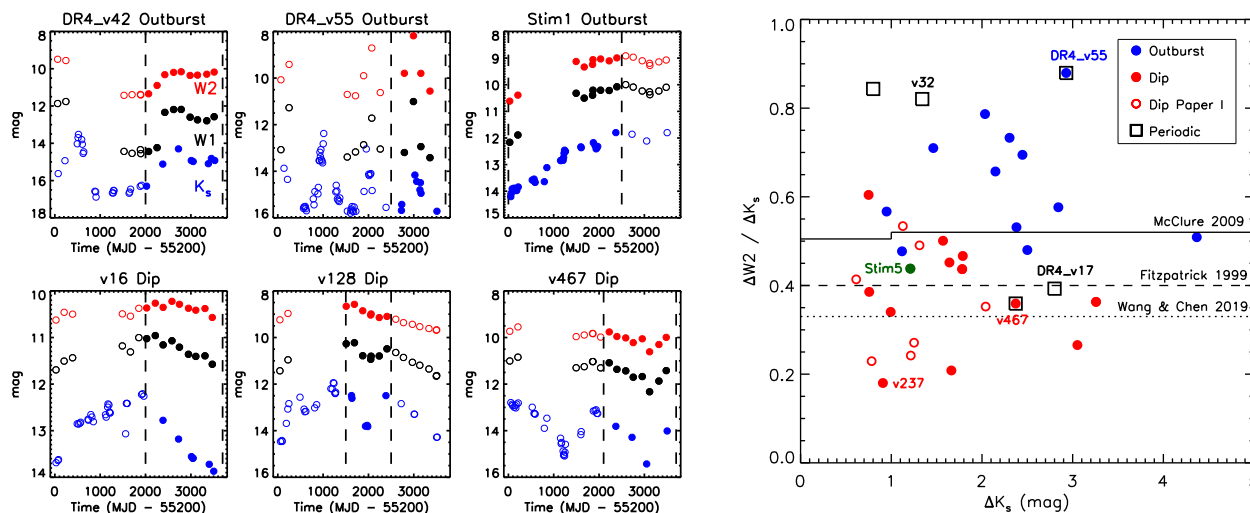
Figure 3. Left: Examples of multiband light curves and visually inspected morphologies. Light curves within the time range of certain dip or outburst are shown by filled circles. The bandpass of the light curves are labelled in the upper left panel. Right: The ratio between $W2$- and K_s-band amplitude of individual events that are classified as dip (red) and outburst (blue). Red open circles represent dips obtained from variable YSO candidates in Paper I. Long-term periodic YSOs are shown by squares. Sinusoidal variables (v32 and DR4_v17) are labelled separately. In addition, Stim5 is marked by the green dot and the amplitudes are measured between two spectroscopic epochs. The $\Delta W2/\Delta K_s$ ratios predicted from analytical ($R_V = 3.1$, Fitzpatrick 1999) and empirical (McClure 2009; Wang & Chen 2019) extinction curves are shown by horizontal lines.

SEDs of most optically bright EXors during the outbursts are well fitted by additional thermal emission from the accretion disc (e.g. Lorenzetti et al. 2012). In other cases, wavelength-dependent flux changes can be used to infer the radial progression of an outburst through the disc, e.g. inward in the case of the recent FUor Gaia 17bpi (Hillenbrand et al. 2018) or outward in the case of WISE 1422-6115 (Lucas et al. 2020). In this section, we use *WISE W*1 (3.4 μm) and *W*2 (4.6 μm) time series photometry from the IRSA archive,[6] taken from the AllWISE MultiEpoch Photometry Table for 2010 (Wright et al. 2010) and the ongoing NEOWISE Reactivation data base from late 2013 onward (Mainzer et al. 2014). There was a 3.5 yr gap between the AllWISE and NEOWISE data. The cadence of the *WISE* light curves is about 180 d (after averaging of the several scans taken over a period of a few days at each epoch). A few examples of the multiband light curves are shown in Fig. 3.

Here, we measure the VVV K_s (ΔK_s) and *WISE W*2 ($\Delta W2$) variations in portions of the light curves of the variable YSOs in our sample, to attempt to distinguish between accretion-driven and extinction-driven changes on time-scales from 1 to 9 yr. From the sample of 61 spectroscopically confirmed YSOs from Paper II and this work, 34 have $W2$-band light curves with long-term photometric variations, including five FUor-like objects. This sample excludes multiple time-scale variables and periodic variables with $P < 700$ d, to avoid sampling issues of low cadence VVV and *WISE* light curves. Almost all of these 34 YSOs are thought to be eruptive variables undergoing episodic accretion. In a few cases this is not proven, e.g.

four (v406, DR4_v15, DR4_v55, and DR4_v67) were classified as having outflow-dominated spectra, though the absence of accretion signatures can be attributed to observation during quiescence in some cases. One additional source DR4_v5 is classified as a Dipper in Table 1 but the spectrum shows clear signatures of a high accretion rate. The K_s, $W1$, and $W2$ light curves of the 34 YSOs are visually inspected and sorted into subgroups where an outburst or a dip can be identified in a certain time window. Examples are shown in Fig. 3. These outbursts or dips are sometimes relatively brief or low in amplitude in comparison to the total variation and the 9 yr light-curve duration. Eruptive YSOs are known to have photometric variations due to extinction as well as episodic accretion, e.g. V1515 Cyg and VSX J205126.1+440523 (Clarke et al. 2005; Kóspál et al. 2011a), so it is not surprising to observe dips within the light curves of eruptive YSOs that could be due to changing extinction.

YSOs without suitable dips or outbursts sampled by the *WISE* and VVV data are excluded from Fig. 3. Periodic variables with sinusoidal light curves are labelled as such since the variation could be equally well regarded as a dip or a burst in many cases. We chose the ratio between K_s and $W2$ amplitudes, instead of between $W1$ and $W2$, to distinguish accretion and extinction driven variations. The wide wavelength range between the K_s and $W2$ bandpasses provides sufficient amplitude differences to measure changing line-of-sight extinction, according to the near- to mid-infrared extinction laws (e.g. Fitzpatrick 1999; McClure 2009). In Fig. 3, we show the measured ΔK_s and $\Delta W2$ for individual dips and outbursts within the time range of the *WISE* data. ΔK_s and $\Delta W2$ are defined within the window of each dip or burst as appropriate. While the VVV and *WISE* measurements are not contemporaneous, the amplitude of these multiyear dips and outbursts is captured fairly well by the data. We therefore have confidence in the overall trends revealed by these metrics even though individual stars are uncertain. In addition, the $\Delta W2/\Delta K_s$ ratio of seven dippers from Paper I is also shown in Fig. 3. These objects are yet to be confirmed as YSOs by spectroscopic follow-up.

---

[6]A few targets lack *WISE* data in the AllWISE and NEOWISE catalogues due to blending. The $W1$ and $W2$ light curves of v14, v621, DR4_v15, DR4_v20, and DR4_v89 were extracted from the time series of unWISE image stacks (unWISE, Lang 2014; Meisner, Lang & Schlegel 2018) by running the CROWDSOURCE crowded field photometry pipeline in an efficient forced photometry mode (Schlafly, Meisner & Green 2019), using the coordinates given in the deep unWISE catalogues available at https://catalog.unwise.me/ which were derived from running CROWDSOURCE on the 5-yr unWISE image stacks (Meisner et al. 2019).
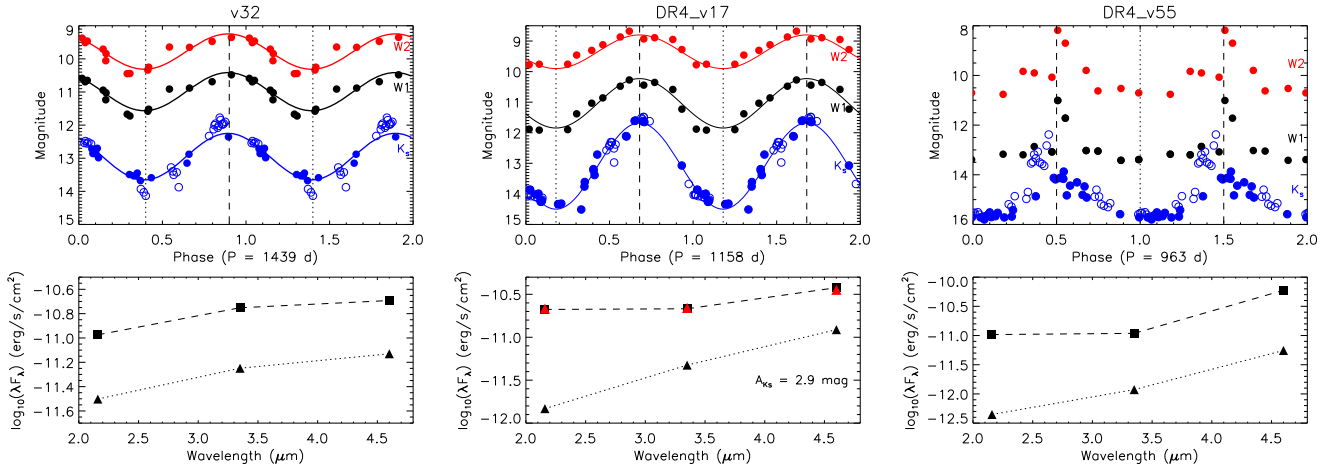
Figure 4. Upper: Phase-folded multiband light curves of three emission line YSOs: v32, DR4_v17, and DR4_v55. K_s data lying outside the time coverage of *WISE* photometry are shown by open circles. Dotted and dashed lines mark out the photometric minimum and maximum. Sinusoidal curves were fit to objects v32 and DR4_v17. Bottom: The three point (K_s, W1, W2) SEDs during photometric maximums (■) and minimums (▲). In the case of DR4_v17, red triangles are overplotted after de-reddening the SED at photometric minimum by $A_{K_s} = 2.9$ mag. We see that the dereddened SED matches the SED measured at photometric maximum. Error bars have similar sizes to the symbols and are therefore not plotted.

All of the 35 sources plotted in Fig. 3 have a bluer-when brighter, redder-when-fainter behaviour in the $K_s - W2$ colour. This behaviour of the infrared colours is typical of optically bright EXors where an outburst takes place in the inner disc, causing it to become hotter and bluer (Lorenzetti et al. 2012). However, Fig. 3 shows that dips and outbursts typically have different $\Delta W2/\Delta K_s$ ratios. Dippers have smaller $\Delta W2/\Delta K_s$ ratios, ranging between 0.18 and 0.50. Several dips with very low $\Delta W2/\Delta K_s$ ratios can be explained by a source of obscuration that hides the near-infrared emitting-region of the disc more than the mid-infrared emitting region. Similar obscuration behaviour was recently observed on a Class II object AA Tau, in which the mid-infrared variation is anticorrelated with optical variation (Covey et al. 2021). By contrast, the $\Delta W2/\Delta K_s$ of most outbursts is larger than 0.4. The boundary between two morphologies, 0.4 and 0.5, is consistent with the infrared extinction laws (e.g. Fitzpatrick 1999; McClure 2009; Wang & Chen 2019). Although some overlap is seen around the boundary, distinct distributions of the $\Delta W2/\Delta K_s$ ratio are seen for dips and outbursts, which can be attributed to changes in extinction and accretion rate, respectively.

Since the VVV and *WISE* light curves were not obtained simultaneously, the measurement of $\Delta W2/\Delta K_s$ for individual YSOs is imprecise, especially for variables with low amplitude or strong variation on a short time-scale. However, colour variations of periodic variables having long periods are more precisely measured in the phase-folded light curves. Fig. 4 presents phase-folded multiband light curves of v32, DR4_v17, and DR4_v55 with their SEDs at photometric minima and maxima measured within the time coverage of the *WISE* light curves. All three objects have emission line spectra, though the CO overtone emission and Br γ emission are relatively weak (or absent in the case of DR4_v55, which shows H_2 emission only). In each case, the spectra were taken in the faint part of the cycle. For DR4_v17, the SED measured at photometric maximum is well reconstructed by applying a de-reddening function to the data taken at the minimum ($A_{K_s} = 2.9$ mag, $R_v = 3.1$, Fitzpatrick 1999). By contrast, DR4_v55 and v32 have similar amplitudes in K_s and in $W2$, indicating their variations are likely linked to accretion bursts modulated by periodic perturbations. For these variable YSOs with periods around 1000 d, the corre-

sponding Keplerian orbital radius is around 2 au for a solar mass star.[7]

The study in this section provides a statistical view of the infrared colour variation of YSOs with variability on long time-scales. Most dippers have greater infrared colour variation, $\Delta(K_s - W2)$, than accretion dominated eruptive YSOs, which is in line with the infrared dust extinction law ($A_{W2}/A_{K_s} = 0.4 - 0.5$). A few YSOs in this work have both variable line-of-sight extinction and variable mass accretion process, so that $\Delta W2/\Delta K_s$ ratios is time dependent. For example, Stim5 (green dot in Fig. 3) began an outburst in 2010 that was ongoing throughout the 9 yr light curve, with $\Delta W2/\Delta K_s = 0.55$. It is therefore classified as an eruptive YSO. However, between 2017 and 2019 there was a dip with $\Delta W2/\Delta K_s = 0.43$. Multi-epoch spectroscopy provides a more reliable interpretation of the variable mechanism: we discuss the variability of Stim5 in Section F.

4.2 Variation time-scales of eruptive YSOs

We now consider the time-scale of accretion-driven outbursts broken down into the different spectroscopic and light-curve categories, in order to gain insight into the physical mechanisms causing these events. As mentioned earlier, the time-scale refers to the total duration of an outburst from the start of the event until the return to quiescence, or to the period in the case of the periodic systems. Later in this section, we also discuss the rise times of the longer duration events. Classical FUor or EXor outbursts have quite distinct duration. Most optical EXor outbursts in the literature lasted less than 1000 d (Herbig 1989), while the three classical FUors have remained in outburst for several decades (Hartmann & Kenyon 1996). In Paper II, the 'MNor' category was tentatively proposed for YSO outbursts of intermediate duration.

Individual objects are placed in the following categories based on their spectra and their light curves.

(i) YSOs with FUor-like spectra.
(ii) Eruptive YSOs with emission-line spectra.

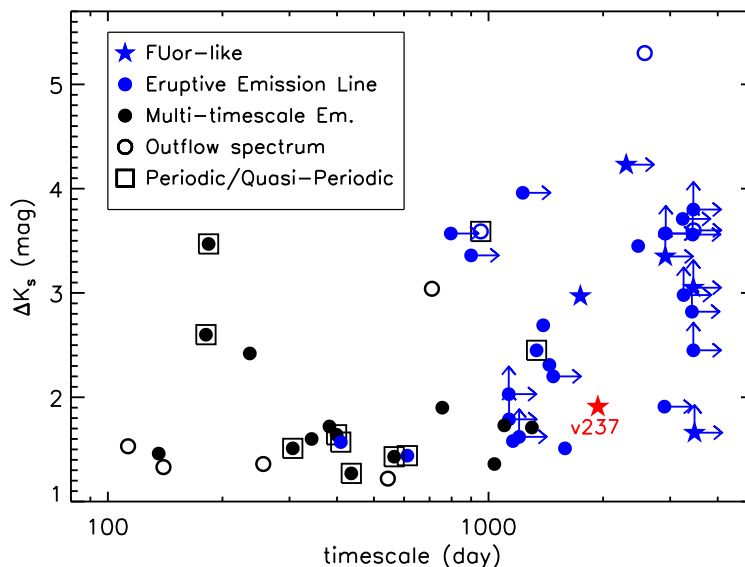[7]$r \sim 2(P/1050\,\mathrm{d})^{2/3}(M_*/M_\odot)^{1/3}$ au.

Figure 5. K_s-band amplitude (ΔK_s) and duration of spectroscopic confirmed eruptive YSOs in the VVV survey. FUor-like YSOs are shown by stars. Emission-line YSOs are shown by circles, including YSOs with eruptive light curve (blue colour), MTV (black colour), YSO with magnetospheric accretion scenario (filled circle), and YSOs with outflow-dominated spectra (open circle). Periodic and quasi-periodic variables are marked by open squares. FUor-like YSO v237 is shown by a red star as its light curve is dominated by extinction dips.

(iii) Multiple time-scale YSOs with emission-line spectra.

(iv) YSOs with outflow-dominated emission-line spectra.

(v) Periodic or quasi-periodic YSOs with emission-line spectra.

For the first three of categories in the list, there is good spectroscopic evidence for accretion-driven outbursts, either from a FUor-like spectrum or from signatures of magnetospheric accretion. The outflow-dominated systems are less clear cut: stars in this category show strong H_2 emission and sometimes [Fe II] emission but lack spectral signatures of magnetospheric accretion or boundary layer accretion. The effect of geometry might play a role on these 'bona-fide outbursts'. In a nearly edge-on system, the emission from the inner disc is heavily obscured while the H_2 emission lines from a jet can dominate the infrared spectrum. The measured line-of-sight extinction of these objects is discussed in Section 4.3 and Appendix E. The timing of the spectroscopy also matters. The three YSOs (DR4_v15, DR4_v55, and DR4_v67) show a long-term outburst in their light curves but have outflow-dominated spectra that were taken during the quiescent state. In Fig. 5, we exclude YSOs that only have dips in light curves attributed to changing extinction, including the periodic variables v467 and DR4_17 (see Section 4.1). Other periodic variables are retained, some of which have clear evidence for accretion-driven variability. The categories of individual YSOs are shown in Table 5.

The duration and ΔK_s values of 52 variable YSOs are presented in Fig. 5. Two variable stars with time-scales around 30 d are not presented (v65 and DR4_v30). The key results are: (i) all six of the FUor-like YSOs have time-scales ≥ 1900 d but (ii) there is no clear separation between them and the emission-line objects in duration or amplitude. In fact, the majority of long duration outbursts show emission-line spectra.

The multiyear-long photometric variations in the FUor-like YSO v237 (marked by red star in Fig. 5) are due to variable line-of-sight extinction rather than changes in accretion rate. Similar variations have been observed in well-studied FUors such as V1515 Cyg (Clarke et al. 2005). Ongoing accretion bursts are seen in two FUor-like YSOs (v721 and DR4_v20) with $\Delta K_s > 3$ mag and $t > 3400$ d. Both the

K_s amplitude and duration of these two FUor-like YSOs are lower limits since their light curves began to rise before the VVV survey started in 2010.

As the only FUor-like YSO where the entire outburst was captured in this work, v322 (see section 4.2.2 in Paper III) exhibited a fast outburst (2.4 mag in 200 d) followed by a rapid initial decay at a rate of 1.56 mag yr^{-1} that then slowed down. The rapid initial decay of v322 is rarely seen among FUor-like YSOs and is comparable to some EXors. One previously discovered 'FUor-like' Class 0 object V371 Ser (also known as EC 53) has similar low amplitude and multiyear photometric behaviour to v322, and it also has H_2 emission lines like v322 (Hodapp et al. 2012; Connelley & Reipurth 2018; Lee et al. 2020).

To investigate the pre-outburst brightness of eruptive objects, we gathered the 2MASS photometry (Skrutskie et al. 2006) from the IRSA online server. The results of individual sources are presented in Appendix D.

4.2.1 MTVs

MTVs were defined in Paper III to have significant variability on short time-scales ($t \sim 50$ d) as well as large interyear variability. In this work, the MTVs are found to be YSOs with similar variation on interyear and intrayear time-scales, and lack of a strong longer term decline or outburst in their VVV light curves. In some cases (e.g. DR4_v30, v181), there are long-term trends in the light curves but their amplitude is smaller than the interyear variation. Many photometric variations of MTVs are only partially captured by the VVV/VVVX light curves due to their sparse sampling. Hence, the variation amplitudes and time-scales of MTVs are highly uncertain. In Fig. 5, we see that most MTVs (except v181) have relatively short time-scales for their interyear variations, consistent with the above definition, and the amplitudes are lower than is seen in most of the longer-time-scale variables.

Among 20 MTVs, five have outflow-dominated spectra, a higher proportion than that found among longer time-scale emission line

Table 5. Final classification and luminosity of eruptive YSOs.

Name	Spectral class	Final classification	Distance (kpc)	L_{IR} log ($L_\odot$)	ΔL_{IR} log ($L_\odot$)	$A^1_{K_s}$ (mag)	$A^2_{K_s}$ (mag)	Time-scale (d)	ΔK_s (mag)	α_{class}
v14	Emission line	Eruptive candidate	1.9^a	0.16	-0.11	0.00	–	398	1.6	0.61
v16	FUor-like	FUor-like	8.2^a	1.84	1.23	0.18	–	3476	1.7	0.07
v20	Emission line	Eruptive with magnetosphere	2.5^c	1.97	1.65	1.40	1.71	1100	1.7	0.47
v32	Emission line	Eruptive with magnetosphere	1.9^a	0.75	0.50	0.49	–	1337	2.5	0.08
v53	Emission line	Eruptive candidate	13.9^a	2.19	1.99	0.00	–	236	2.4	0.61
v63	Emission line	Eruptive candidate	3.5^b	0.74	0.36	0.89	–	136	1.5	-0.24
v65	Emission line	Eruptive candidate	3.5^b	1.08	0.80	1.00	–	30	1.4	-0.27
v94	Emission line	Eruptive with magnetosphere	3.5^b	1.56	1.29	0.00	–	436	1.3	0.17
v118	Emission line	Eruptive candidate	2.2^c	0.91	0.88	0.19	–	50	3.5	0.12
v128	Emission line	Eruptive with magnetosphere	2.6^b	1.30	1.06	>1.00	–	1131	1.8	0.56
v181	Emission line	Eruptive candidate	–	–	–	0.79	–	183	3.5	0.58
v190	Emission line	Eruptive candidate	4.0^a	1.25	0.57	1.28	2.50	612	1.4	-0.43
v193	Emission line	Non-eruptive	4.5^a	1.92	1.79	>2.01	–	763	1.4	0.35
v237	FUor-like	Pre-VVV-eruptive?	5.0^a	1.91	1.34	>0.96	–	1943	1.9	0.88
v270	Emission line	Eruptive with magnetosphere	4.6^a	1.79	1.61	1.55	–	3237	3.7	0.87
v309	Emission line	Eruptive with magnetosphere	2.8^a	2.35	1.99	>1.42	1.45	181	2.6	1.30
v322	FUor-like	FUor-like	3.8^a	–	–	0.45	–	1743	3.0	0.82
v335	Emission line	Non-eruptive	4.2^a	1.86	1.51	0.71	–	1041	3.6	0.45
v374	Emission line	Eruptive with magnetosphere	2.9^b	2.47	2.02	1.04	–	3254	3.0	0.56
v376	Emission line	Eruptive with magnetosphere	1.2^a	-0.04	-0.37	0.90	–	1300	1.7	-0.37
v389	Emission line	Eruptive with magnetosphere	4.3^a	1.80	1.46	>0.91	–	1036	1.4	0.68
v405	Emission line	Non-eruptive	2.3^b	1.85	1.64	>0.15	–	733	2.2	1.10
v406	Outflow	Non-eruptive	2.3^b	1.57	1.25	0.92	–	796	1.7	0.80
v452	Emission line	Eruptive with magnetosphere	2.8^c	1.12	1.05	0.82	–	2472	3.5	0.21
v467	Emission line	Non-eruptive (periodic)	9.0^a	1.86	1.58	0.98	–	1840	2.6	-0.27
v473	Outflow	Outflow dominated	3.7^b	1.69	1.21	–	2.21	113	1.5	0.89
v480	Emission line	Eruptive candidate	3.7^b	0.30	-0.07	0.00	–	306	1.5	-0.81
v562	Emission line	Eruptive with magnetosphere	2.9^b	0.97	0.82	0.96	–	1392	2.7	-0.02
v618	Outflow	Outflow dominated	–	–	–	0.77	1.29	140	1.3	-0.09
v621	Emission line	Eruptive with magnetosphere	–	–	–	1.26	–	2898	1.9	-0.05
v625	Emission line	Eruptive candidate	2.3^b	0.64	0.41	>0.00	–	343	1.6	0.17
v628	Outflow	Outflow dominated	2.3^a	–	–	0.45	–	256	1.4	-0.47
v630	Emission line	Eruptive with magnetosphere	1.9^a	–	–	0.95	–	409	1.6	2.70
v631	Emission line	Eruptive with magnetosphere	2.3^b	1.61	1.52	0.73	–	3422	2.8	0.62
v632	Emission line	Eruptive candidate	2.5^b	1.32	0.84	0.14	–	382	1.7	-0.05
v636	Emission line	Eruptive candidate	2.8^b	1.07	0.77	1.19	–	565	1.4	0.43
v662	Emission line	Eruptive with magnetosphere	3.1^b	1.11	0.82	>0.00	–	1159	1.6	0.53
v665	Emission line	Eruptive with magnetosphere	4.3^a	1.93	1.44	1.41	–	1203	1.6	0.58
v699	Emission line	Eruptive with magnetosphere	4.9^a	1.87	1.26	>1.05	1.94	756	1.9	0.91
v713	Emission line	Eruptive with magnetosphere	3.5^a	1.58	1.40	0.19	–	1130	2.0	-0.04
v717	FUor-like	FUor-like	6.1^a	2.16	1.77	1.63	–	2300	4.2	0.23
v721	FUor-like	FUor-like	4.9^a	1.98	1.80	0.85	–	3452	3.0	0.55
v800	Emission line	Eruptive with magnetosphere	1.4^b	2.45	2.36	1.18	–	1479	2.2	0.94
v815	Outflow	Outflow dominated	3.1^b	1.28	0.87	–	0.48	544	1.2	1.08
Stim1	Emission line	Eruptive with magnetosphere	10.5^a	2.47	2.35	0.40	–	3452	2.5	0.63
Stim5	Emission line	Eruptive with magnetosphere	5.1^a	1.41	1.33	0.92	0.44	3452	3.8	0.90
Stim13	Emission line	Eruptive with magnetosphere	2.7^a	2.73	1.61	>0.40	1.22	1588	1.5	1.33
DR4_v5	Emission line	Eruptive with magnetosphere	1.8^a	1.23	0.69	1.14	–	1230	4.0	0.96
DR4_v10	Emission line	Eruptive with magnetosphere	4.2^a	0.87	0.57	>1.06	–	3437	3.6	1.86
DR4_v15	Outflow	Outflow dominated	4.3^b	2.21	2.04	–	3.29	3456	3.6	0.56
DR4_v17	Emission line	Non-eruptive (periodic)	4.3^a	1.92	1.79	1.05	–	1155	3.8	0.78
DR4_v18	Emission line	Eruptive with magnetosphere	5.2^a	1.68	1.60	0.54	–	796	3.6	0.21
DR4_v20	FUor-like	FUor-like	4.7^a	1.02	0.78	>0.60	–	2913	3.3	0.74
DR4_v30	Emission line	Eruptive candidate	6.7^a	2.31	2.21	1.02	–	30	3.9	0.36
DR4_v34	Emission line	Eruptive with magnetosphere	4.0^a	1.94	1.17	1.30	–	2904	3.6	-0.19
DR4_v39	Emission line	Eruptive with magnetosphere	4.6^a	1.55	1.30	0.90	1.16	1445	2.3	0.51
DR4_v42	Emission line	Eruptive with magnetosphere	6.6^a	1.84	1.74	>0.07	1.11	900	3.4	1.26
DR4_v44	Emission line	Eruptive with magnetosphere	3.9^a	1.17	0.89	>1.05	–	2921	3.6	0.83
DR4_v55	Outflow	Outflow dominated	3.4^b	3.04	2.99	–	3.79	954	3.6	1.97
DR4_v67	Outflow	Outflow dominated	4.5^b	2.01	1.94	1.20	1.19	2572	5.3	1.05
DR4_v89	Outflow	Outflow dominated	2.3^b	1.49	0.93	–	2.39	710	3.0	0.85

Notes. 'Eruptive candidate' represents a YSO with eruptive spectrum but also lack of a significant long-term variation.

A_{K_s} measured by the location on near-infrared colour–colour diagram.

A_{K_s} measured by the flux ration between the H_2 1–0 Q(3) and 1–0 S(1) emission.

^{a}Kinematic distance measured by the radial velocity of emission features.

^{b}Distance estimated by the nearby star-forming regions. ^{c}Distance estimated from the SED fitting in Paper II.

YSOs (2/30). It is not a very surprising result because MTVs lack of major outbursts that lead to emission features like Br γ and CO band heads. The variable nature of outflow-dominated sources are likely linked to inner disc structures, either resulting from unstable mass accretion or variable line-of-sight extinction. Six MTVs have quasi-periodic variations. The spectral indices of MTVs are similar to longer time-scale variables, as $-0.37 < \alpha_{class} < 1.30$. Most of these MTVs are listed as 'eruptive candidates' in Table 5 as no major (long-term) eruptive event was observed.

4.3 Extinction and luminosity measurements

In this work, the line-of-sight extinctions (A_{K_s}) of YSOs are measured by two methods, either by their locations on the near-infrared colour–colour diagram or by the flux ratio between H_2 1–0 Q(3) (2.42 μm) and 1–0 S(1) (2.12 μm) lines, where possible. The details of two measurement methods and further discussions are presented in Appendix E. The measured A_{K_s} from both methods are listed in Table 5. One should notice that the measured A_{K_s} is the integrated extinction along the line of sight to the star, including interstellar extinction between the sun to the star-forming region, the extinction within the molecular cloud and the circumstellar extinction.

Nine YSOs in the sample have outflow-dominated spectra. The A_{K_s} value is measured for all nine YSOs, mostly by the H_2 flux ratio, five of the nine have intermediate extinction, and four have A_{K_s} ranging from 2.20 to 3.79 mag, significantly higher than the extinction found in other emission-line objects measured by both methods. We infer that in erupting systems where Br γ and CO overtone emission are not seen, this is sometimes due to heavy obscuration of the inner regions of the system. This suggests that high disc inclination is playing a role (i.e. close to edge-on orientation). Evolutionary stage may also be a factor but the spectral indices of the four highly extinguished outflow-dominated sources span a wide range ($\alpha_{SED} = 0.11, 0.33, 1.56$ for DR4_v89, DR4_v15 and DR4_v55, respectively, while v473 lacks a $W4$ detection).

The in-outburst infrared luminosity (L_{IR}) and the rise in luminosity from the quiescent state (ΔL_{IR}) of eruptive YSOs are measured using the extinction-corrected 2–22 μm SED. The extinction correction is conducted based on the A_{K_s} value measured above, in which the H_2 line ratio method is preferred, and the empirical near-to-mid-infrared extinction law is from McClure (2009). For preference, the distances used in the calculation are radial-velocity-based kinematic distances (d_k, listed in Table 2) and the distance ambiguity is broken using the VIRAC2 proper motions (see Section 2.5). Where d_k is unavailable, we use the distance to the star-forming region (d_{SFR}) given in Table 1 or the distance determined in Paper II.[8] To measure the quiescent luminosity, we use the K_s and $W1$ to $W4$ magnitudes from VVV and ALLWISE, these data being taken in 2010 when the sources were in a faint state. To calculate the in-outburst luminosity, L_{IR}, we use the K_s, $W1$, and $W2$ magnitudes measured in the bright state. The mid-infrared luminosity increased during outburst can be affected by many mechanisms (MacFarlane et al. 2019) so we estimate the in-outburst $W3$ and $W4$ magnitudes by assuming that the $W2$-$W3$ and $W3$-$W4$ colours measured in the ALLWISE survey remain constant while the $W2$ flux increases. Luminosity is not calculated for YSOs lacking $W3$ and $W4$ detections in ALLWISE, such as the FUor-like source v322. This leaves us with L_{IR} values for five FUor-like
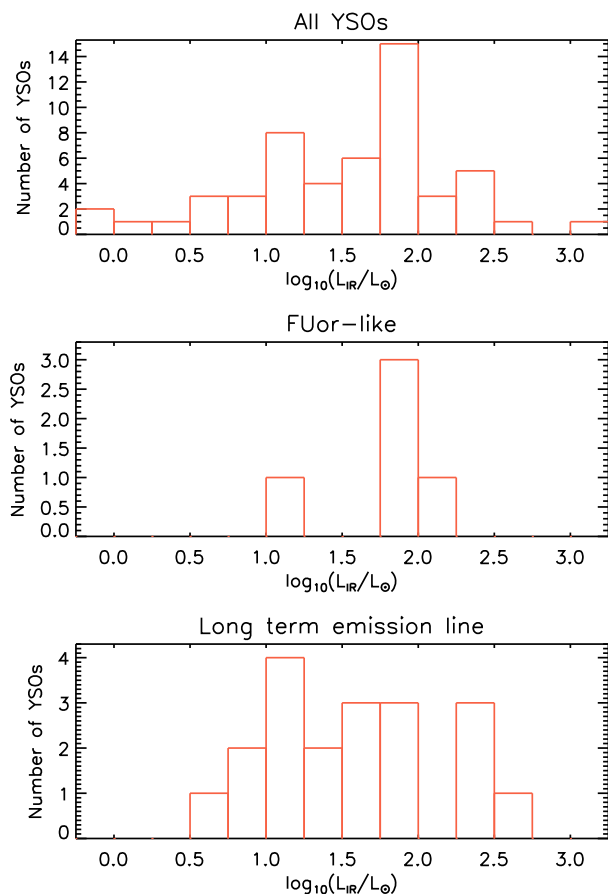

Figure 6. Histograms of the infrared luminosity (L_{IR}, between 2 and 22 μm) of YSOs in this work. All YSOs, FUor-like objects, and eruptive YSOs with emission-line spectra are presented separately. YSOs lack of *WISE* detections are not shown in this figure.

YSOs. In a few systems the luminosity is a lower limit because the extinction value, A_{K_s}, is a lower limit. These luminosity calculations are obviously uncertain but they allow us to make comparisons between FUor-like YSOs and emission-line YSOs in the sample and eruptive YSOs in the literature.

The distribution of L_{IR} of FUor-like objects and eruptive YSOs with emission-line spectra is presented in Fig. 6. In our sample, FUor-like objects have L_{IR} ranging from 10 to 143 L$_\odot$, which is similar to previously identified FUors (e.g. Connelley & Reipurth 2018). Long-term eruptive emission-line YSOs have a similar range of luminosities to the FUor-like YSOs. In many sources, the quiescent luminosity is not measured, e.g. if the source was in outburst in 2010. However, the rise in luminosity, ΔL_{IR}, is approximately equal to L_{IR}, the in-outburst luminosity, where this is measured. L_{IR} is therefore a rough estimate of the accretion luminosity during the bright state in the measured wavelength range.[9]

In long-term magnetospheric accretion controlled outbursts, L_{IR} is typically 10^1–10^2 L$_\odot$. This is a little higher than many previously discovered EXors in nearby star-forming regions, such as EX Lupi (Aspin et al. 2010) and others (Lorenzetti et al. 2012). This is likely to be a selection effect, owing to the larger distances to the YSOs

---

[8]We exclude v621 from this measurement due to its unknown distance. The d_k value, based on the Br γ line, disagrees with the PM solution. No distance has been published for the star forming region.

[9]In Paper II, the accretion luminosity of emission line YSOs was estimated using $L_{Br \gamma}$, which was strongly model dependent and could be heavily biased by the veiling effect from the continuum.

presented here. Our results indicate that accretion rates are typically of the same order for the boundary layer mode and the magnetospheric mode in embedded Class I YSOs. This contrasts with nearby optically visible systems where EXors typically have lower luminosities and accretion rates than FUors. The measured extinctions, luminosities, and classifications of the 61 spectroscopically confirmed YSOs are listed in Table 5.

4.4 Classification

In this section, we refine the classification of eruptive YSOs based on their photometric and spectroscopic features. In Paper II, 'MNor' was defined as a tentative subgroup of eruptive YSOs. 'MNors' have mixed characteristics of classical EXors and classical FUors, and with Class I or flat-spectrum SEDs. In terms of outburst duration (often intermediate, i.e. 1–5 yr) or spectral features (emission or absorption), 'MNors' are opposite to those expected from the outburst time-scale. Under this definition, 'MNor' contains both emission-line YSOs having outbursts longer than typical 'EXors' and FUor-like objects without decades-long photometric eruptions. Among eruptive YSOs in the VVV survey, we found that 'MNors' are more common than either 'FUors' or 'EXors' among eruptive YSOs with a large variety of duration and amplitude. The term is therefore not especially useful, except to highlight that the FUor/EXor categories defined for optically bright systems cannot encompass what is seen in embedded systems. Hence, in this work, eruptive YSOs are sorted by accretion mode and light-curve properties instead of traditional categories. The category of FUors is fairly well defined by their unique spectral features, long duration, and the outburst luminosity, while there are some differences in the rise time of individual objects. On the other hand, we favour 'emission-line objects' to 'EXors' owing to the wide range in duration of eruptive events controlled by the magnetospheric accretion mode. The final classification is presented in Table 5.

Among the 16 variables with the longest duration ($t > 2000$ d) in our sample, nine have indicators of the magnetospheric accretion process and two are dominated by outflows. We considered whether this result might be affected by disc orientation. Discs viewed close to face-on (i.e. at small inclinations) are more likely to display emission-line features arising in the innermost disc and in magnetospheric accretion columns, whereas these can be hidden from view at high inclinations. We do not see significantly lower extinction in emission line objects than FUor-like sources, which indicates that our result is not strongly biased by the disc orientation (see Section E). We conclude that magnetospheric accretion can be maintained during long-duration outbursts and that this is more common than boundary layer accretion in Class I YSOs.

Both slow-rising and fast-rising outbursts were observed among emission line objects. Slow-rising eruptive YSOs (e.g. Stim1 and DR4_v15) are possibly triggered by thermal instability where the instability is formed at the inner disc without a dynamical perturbation and then propagates inside-out (Lin, Papaloizou & Faulkner 1985; Bell & Lin 1994). On the other hand, outbursts with fast eruptive nature (e.g. v621 and DR4_v34) could be consequences of disc fragments being accreted on to the protostar (e.g. Vorobyov & Basu 2006).

4.5 AGB stars and symbiotic systems: v51, v319, and v370

In this work, we identified three AGB stars via the ^{12}CO and ^{13}CO absorption bands. Notably, two AGB stars, v319 and v370, exhibit both Br γ emission and CO absorption. In addition, the WISE *W*1-*W*2 colours of these two stars are bluer than solitary AGB stars. We

hereby identify v319 and v370 as D-type symbiotic stars (e.g. Kenyon & Webbink 1984; Corradi et al. 2008). More detailed description of these three AGB stars is provided in Appendix G.

5 SUMMARY AND CONCLUSIONS

In this work, we report results of spectroscopic follow-up for 38 high amplitude variable stars ($\Delta K_s > 1$ mag) discovered in the VVV survey, including 33 that are spectroscopically confirmed as YSOs. We add them to the sample of 28 confirmed YSOs from Paper II for a combined sample of 61 highly variable YSOs. Based on spectral index, 56 of them are Class I and flat-spectrum objects. We publish the VIRAC2 version of the VVV K_s light curves from 2010 to 2019 for all 61 VVV YSOs (available in the online supplemental material, examples in Table B1). The sample includes some YSOs with long duration outbursts (typically 2–4 mag amplitude), some with periodic variability, some MTVs and some with extinction-dominated variability. There are also a few post-main-sequence variable stars.

Our main findings are as follows.

(i) Spectroscopically, the 61 variable YSOs are sorted as 55 emission-line YSOs and 6 FUor-like objects. Among emission-line YSOs, 46 sources display emission features linked to the magnetospheric accretion process (Pa β or Br γ) usually accompanied by CO overtone emission and sometimes Na I emission. The remaining nine emission-line sources show only lines associated with a molecular outflow or disc wind (H$_2$ or [Fe II]). The FUor-like objects have ^{12}CO overtone absorption bands and water absorption in the *H* and K_s bandpasses, associated with the boundary layer accretion process.

(ii) The dominant time-scales of variability seen in the YSO sample range from months to a decade for different sources. FUor-like spectra are only seen during outburst events with duration $\geq$5 yr.

(iii) Signatures of magnetospheric accretion were observed among most eruptive YSOs with long duration outbursts. Therefore, the stellar magnetic field is still in control during these outbursts, which have similar infrared amplitudes and luminosities to the FUor-like sources. This contrasts with past results for long duration optically selected events, where FUor-like spectra are almost always seen (e.g. Audard et al. 2014). There is no clear difference in the measured extinction for the two spectral categories, indicating that the spectral classification is not driven primarily by the disc inclination angle and veiling.

(iv) Similar in-outburst luminosities were seen among emission-line and FUor-like eruptive YSOs that suggest that they may have similar accretion rates.

(v) Periodic accretors comprise a significant minority amongst eruptive protostars. Using the Lomb–Scargle method, photometric periods are detected in several emission-line YSOs, though three or four of these require more data to confirm or disprove the periodic behaviour. For the four longest period systems ($P > 950$ d), two systems are periodic accretors and two systems as cases of periodic extinction identified by the $\Delta W2/\Delta K_s$ colour ratio. While a determination could not be made for the other nine quasi-periodic YSOs. The finding of periodic accretors suggests that an orbiting companion or star–disc interactions are be able to modify the mass accretion rate. At present, the two cyclically accreting YSOs, v32 and DR4_v55, only have spectra taken in the quiescent state, where relatively weak CO overtone and Br γ emission features were observed comparing to other eruptive spectra taken in outburst. Multiple epochs of spectroscopy and multiwavelength photometry

will be needed to study the cyclical accretion and to distinguish between accretion and extinction in the other periodic systems.

(vi) MTVs have relatively short duration outbursts ($<$1–3 yr). First noted in Paper III as YSOs that vary strongly on time-scales of weeks and years, these systems show repeated bursts or dips and they have typical amplitudes below 2 mag in K_s. The rapid component of the variability is likely linked to an unstable accretion process, star–disc interactions, or inner disc structures causing variable extinction. By contrast, frequent intrayear high amplitude variations are not often seen among long-term eruptive YSOs.

(vii) Variable line-of-sight extinction contributes to the photometric variation in a few sources. Such changes are sometimes seen on the 'bright plateau' in the light curve of eruptive YSOs (e.g. Stim5). The extinction dips are recognized by light-curve morphologies and are further identified by a smaller $\Delta W2/\Delta K_s$ ratio than is seen in outbursts. As noted above, the long period variability in two of the emission-line YSOs is extinction driven, presumably by asymmetric disc structures. The light curve of one FUor-like source, v237, is also dominated by extinction dips in the 2010–2019 time interval. The combined 2MASS and VVV light curve suggests that v237 has been in a high state of accretion for at least two decades.

(viii) In this work, five sources are identified as post-main-sequence stars. The quasi-periodic variable v371 is a newly discovered Wolf–Rayet star in a binary system, which is named as WR80-1 in accordance with the naming convention. Two AGB stars with periodic/quasi-periodic light curves are classified as D-type symbiotic stars with Br γ emission features arising from the accretion process of their companion stars.

DATA AVAILABILITY

The *WISE*, *Spitzer*, and 2MASS data underlying this article are publicly available at https://irsa.ipac.caltech.edu/Missions/wise.html, https://irsa.ipac.caltech.edu/Missions/spitzer.html, and https://irsa.ipac.caltech.edu/Missions/2mass.html respectively. The VVV and VVVX data are publicly available at the ESO archive http://archive.eso.org/cms.html. The relevant reduced products for the most recent VVVX epochs have not yet been publicly released but are available on request to the first author. The lasted VVV/VVVX K_s-band light curves of the spectroscopic follow-up samples are provided in Table B1. The reduced spectra are provided at http://star.herts.ac.uk/~pwl/Lucas/GuoZ/VVVspec/.

REFERENCES

Alcalá J. M. et al., 2014, A&A, 561, A2
Allers K. N. et al., 2007, ApJ, 657, 511
Alonso-García J., Mateo M., Sen B., Banerjee M., Catelan M., Minniti D., von Braun K., 2012, AJ, 143, 70
Aspin C. et al., 2009, ApJ, 692, L67
Aspin C., Reipurth B., Herczeg G. J., Capak P., 2010, ApJ, 719, L50
Audard M. et al., 2010, A&A, 511, A63
Audard M., et al., 2014, Protostars and Planets VI. University of Arizonal Press, Chicago, IL, USA, p. 387
Bell K. R., Lin D. N. C., 1994, ApJ, 427, 987
Benjamin R. A. et al., 2003, PASP, 115, 953
Bensby T. et al., 2013, A&A, 549, A147
Bouvier J. et al., 2007, A&A, 463, 1017
Carey S. J. et al., 2009, PASP, 121, 76
Chené A.-N., St-Louis N., 2010, ApJ, 716, 929
Chrysostomou A., Bacciotti F., Nisini B., Ray T. P., Eislöffel J., Davis C. J., Takami M., 2008, A&A, 482, 575
Clarke C., Lodato G., Melnikov S. Y., Ibrahimov M. A., 2005, MNRAS, 361, 942
Connelley M. S., Greene T. P., 2010, AJ, 140, 1214
Connelley M. S., Reipurth B., 2018, ApJ, 861, 145
Contreras Peña C. et al., 2017a, MNRAS, 465, 3011 (Paper I)
Contreras Peña C. et al., 2017b, MNRAS, 465, 3039 (Paper II)
Contreras Peña C., Naylor T., Morrell S., 2019, MNRAS, 486, 4590
Corradi R. L. M. et al., 2008, A&A, 480, 409
Covey K. R., Larson K. A., Herczeg G. J., Manara C. F., 2021, AJ, 161, 61
D'Angelo C. R., Spruit H. C., 2010, MNRAS, 406, 1208
D'Angelo C. R., Spruit H. C., 2012, MNRAS, 420, 416
Dahm S. E., Hillenbrand L. A., 2020, AJ, 160, 278
Davies B., Lumsden S. L., Hoare M. G., Oudmaijer R. D., de Wit W.-J., 2010, MNRAS, 402, 1504
Dunham J. L., 1932, Phys. Rev., 41, 721
Dunham M. M., Vorobyov E. I., 2012, ApJ, 747, 52
Farrenq R., Guelachvili G., Sauval A. J., Grevesse N., Farmer C. B., 1991, J. Mol. Spectrosc., 149, 375
Fehér O., Kóspál Á., Ábrahám P., Hogerheijde M. R., Brinch C., 2017, A&A, 607, A39
Fitzpatrick E. L., 1999, PASP, 111, 63
Freudling W., Romaniello M., Bramich D. M., Ballester P., Forchi V., García-Dabló C. E., Moehler S., Neeser M. J., 2013, A&A, 559, A96
Gagne J., Lambrides E., Faherty J. K., Simcoe R., 2015, FireHose v2: Firehose v2.0
Green J. D. et al., 2013, ApJ, 772, 117
Greene T. P., Lada C. J., 1996, AJ, 112, 2184
Greene T. P., Lada C. J., 2002, AJ, 124, 2185
Greene T. P., Barsony M., Weintraub D. A., 2010, ApJ, 725, 1100

Großschedl J. E. et al., 2019, A&A, 622, A149
Guo Z. et al., 2018a, ApJ, 852, 56
Guo Z., Gully-Santiago M., Herczeg G. J., 2018b, ApJ, 868, 143
Guo Z. et al., 2020, MNRAS, 492, 294 (Paper III)
Gutermuth R. A., Heyer M., 2015, AJ, 149, 64
Hajdu G., Dékány I., Catelan M., Grebel E. K., 2020, Exp. Astron., 49, 217
Hartmann L., Kenyon S. J., 1996, ARA&A, 34, 207
Hartmann L., Zhu Z., Calvet N., 2011, preprint (arXiv:1106.3343)
Hartmann L., Herczeg G., Calvet N., 2016, ARA&A, 54, 135
Herbig G. H., 1989, in Reipurth B., ed., ESO Workshop on Low Mass Star Formation and Pre-Main Squence Objects, Vol. 33, Garching bei Munchen: European Southern Observatory, p. 233
Herbig G. H., 2008, AJ, 135, 637
Hillenbrand L. A. et al., 2018, ApJ, 869, 146
Hodapp K. W., Chini R., Watermann R., Lemke R., 2012, ApJ, 744, 56
Hodapp K. W. et al., 2020, AJ, 160, 164
Ilee J. D. et al., 2013, MNRAS, 429, 2960
Johns-Krull C. M., Valenti J. A., 2001, ApJ, 561, 1060
Jose J. et al., 2020, ApJ, 892, 122
Kausch W. et al., 2015, A&A, 576, A78
Kenyon S. J., Webbink R. F., 1984, ApJ, 279, 252
Kenyon S. J., Hartmann L. W., Strom K. M., Strom S. E., 1990, AJ, 99, 869
Kenyon S. J., Kolotilov E. A., Ibragimov M. A., Mattei J. A., 2000, ApJ, 531, 1028
Kóspál Á. et al., 2011a, A&A, 527, A133
Kóspál Á. et al., 2011b, ApJ, 736, 72
Kóspál Á. et al., 2016, A&A, 596, A52
Kóspál Á., Szabó Zs. M., Ábrahám P., Kraus S., Takami M., Lucas P. W., Contreras Peña C., Udalski A., 2020, ApJ, 889, 148
Kraus M., Krügel E., Thum C., Geballe T. R., 2000, A&A, 362, 158
Lada C. J., 1987, in Peimbert M., Jugaku J., eds, Proc. IAU Symp. 115, Star Forming Regions. Kluwer, Dordrecht, p. 1
Lang D., 2014, AJ, 147, 108
Lee Y.-H. et al., 2020, ApJ, 903, 5
Lin D. N. C., Papaloizou J., Faulkner J., 1985, MNRAS, 212, 105
Lodato G., Clarke C. J., 2004, MNRAS, 353, 841
Lorenzetti D., Larionov V. M., Giannini T., Arkharov A. A., Antoniucci S., Nisini B., Di Paola A., 2009, ApJ, 693, 1056
Lorenzetti D. et al., 2012, ApJ, 749, 188
Lucas P. W., Roche P. F., Allard F., Hauschildt P. H., 2001, MNRAS, 326, 695
Lucas P. W. et al., 2017, MNRAS, 472, 2990
Lucas P. W. et al., 2020, MNRAS, 499, 1805
McClure M., 2009, ApJ, 693, L81
MacFarlane B., Stamatellos D., Johnstone D., Herczeg G., Baek G., Chen H.-R. V., Kang S.-J., Lee J.-E., 2019, MNRAS, 487, 4465
Mainzer A. et al., 2014, ApJ, 792, 30
Mauerhan J. C., Van Dyk S. D., Morris P. W., 2009, PASP, 121, 591
Meisner A. M., Lang D., Schlegel D. J., 2017, AJ, 153, 38
Meisner A. M., Lang D. A., Schlegel D. J., 2018, Res. Notes Am. Astron. Soc., 2, 202
Meisner A. M., Lang D., Schlafly E. F., Schlegel D. J., 2019, PASP, 131, 124504
Meyer M. R., Calvet N., Hillenbrand L. A., 1997, AJ, 114, 288
Minniti D., 2016, Proceedings of the conference "Galactic Surveys: New Results on Formation, Evolution, Structure and Chemical Evolution of the Milky Way", Sesto, Italy, p. 10
Minniti D. et al., 2010, New Astron., 15, 433
Muzerolle J., Hartmann L., Calvet N., 1998, AJ, 116, 455

Muzerolle J., Furlan E., Flaherty K., Balog Z., Gutermuth R., 2013, Nature, 493, 378
Naik S., Banerjee D. P. K., Ashok N. M., 2009, MNRAS, 394, 1551
Najita J., Carr J. S., Tokunaga A. T., 1996, ApJ, 456, 292
Pecaut M. J., Mamajek E. E., 2013, ApJS, 208, 9
Rebull L. M., Stauffer J. R., Cody A. M., Hillenbrand L. A., David T. J., Pinsonneault M., 2018, AJ, 155, 196
Reid M. J. et al., 2014, ApJ, 783, 130
Rosslowe C. K., Crowther P. A., 2015, MNRAS, 447, 2322
Saito R. K. et al., 2012, A&A, 537, A107
Schechter P. L., Mateo M., Saha A., 1993, PASP, 105, 1342
Schlafly E. F., Meisner A. M., Green G. M., 2019, ApJS, 240, 30
Shu F. H., 1977, ApJ, 214, 488
Simcoe R. A. et al., 2013, PASP, 125, 270
Skrutskie M. F. et al., 2006, AJ, 131, 1163
Smette A. et al., 2015, A&A, 576, A77
Smith L. C. et al., 2018, MNRAS, 474, 1826
Stellingwerf R. F., 1978, ApJ, 224, 953
Venturini C. C., Rudy R. J., Lynch D. K., Mazuk S., Puetter R. C., 2004, AJ, 128, 405
Vernet J. et al., 2011, A&A, 536, A105
Vorobyov E. I., Basu S., 2005, ApJ, 633, L137
Vorobyov E. I., Basu S., 2006, ApJ, 650, 956
Vorobyov E. I., Basu S., 2010, ApJ, 719, 1896
Wang S., Chen X., 2019, ApJ, 877, 116
Wenger T. V., Balser D. S., Anderson L. D., Bania T. M., 2018, ApJ, 856, 52
Wheelwright H. E., Oudmaijer R. D., de Wit W. J., Hoare M. G., Lumsden S. L., Urquhart J. S., 2010, MNRAS, 408, 1840
Williams P. M., 2019, MNRAS, 488, 1282
Wright E. L. et al., 2010, AJ, 140, 1868
Zechmeister M., Kürster M., 2009, A&A, 496, 577
Zhu Z., Hartmann L., Calvet N., Hernandez J., Muzerolle J., Tannirkulam A.-K., 2007, ApJ, 669, 483
Zhu Z., Espaillat C., Hinkle K., Hernandez J., Hartmann L., Calvet N., 2009a, ApJ, 694, L64
Zhu Z., Hartmann L., Gammie C., 2009b, ApJ, 694, 1045

SUPPORTING INFORMATION

Supplementary data are available at *MNRAS* online.

Figure S1. The VIRAC2b version of the K_s-band light curves from the VVV survey.

Figure S2. 2MASS and VVV K_s-band light curves of long-term variable YSOs. The spectroscopic category of individual object is labelled on the plots.

Figure S3. Extinction versus outburst duration. A_{K_s} measurements using the colour–colour diagram are shown in black, while measurements via the H_2 line flux ratio are shown by red.

Figure S4. Spectra of Stim5 in 2017 and 2019 epochs. Left: normalized K_s-band spectra of Stim5.

Table_F1.txt.
Table_G1.txt.
Table_G2.txt.

Please note: Oxford University Press is not responsible for the content or functionality of any supporting materials supplied by the authors. Any queries (other than missing material) should be directed to the corresponding author for the article.

APPENDIX A: VARIABLE YSOS DISCOVERED BY W. STIMSON

In Paper I, the co-author W. Stimson carefully searched two VVV disc tiles (d064 and d083) for highly variable stars ($\Delta K_s \geq 1$ mag) in order to estimate the completeness of the larger search in that work, where strict data quality criteria were used. The search by Stimson found 14 variable stars that were not in the list of 816 variable sources published in Paper I (listed in Table A1). Spectra for three of these variable stars, Stim1, Stim5, and Stim13, are presented in this work. No details of these 14 stars were given in Paper I so we list here their coordinates and

Table A1. Details of the 14 variable stars found by Stimson.

Name	RA	Declination	Class	Light-curve properties
Stim1	12:57:44.23	−62:15:06.4	YSO	Eruptive
Stim2	12:58:29.27	−61:47:25.0	YSO	Eruptive
Stim3	13:05:30.03	−62:29:18.7	YSO	STV
Stim4	13:06:37.34	−62:35:04.3	YSO	Dipper
Stim5	16:12:14.41	−51:50:24.4	YSO	Eruptive
Stim6	16:13:12.28	−51:39:03.7	YSO	Dipper, MTV
Stim7	16:14:45.48	−50:57:49.0	YSO	Fader, MTV
Stim8	16:14:51.45	−51:45:41.9	AGB	$P = 860$ d
Stim9	16:16:08.12	−51:41:31.5	AGB	$P = 591$ d
Stim10	16:16:13.16	−51:03:56.8	EB	$P = 1.22058$ d
Stim11	16:17:32.79	−51:16:55.9	YSO	Eruptive, MTV
Stim12	16:17:59.50	−51:57:05.7	YSO	Dipper, MTV
Stim13	16:19:10.80	−51:03:53.0	YSO	Dipper
Stim14	16:21:42.16	−51:23:29.6	Microlensing	–

classifications. We use the abbreviation 'Stim' to distinguish these variable stars from sources found in our other searches. The classifications draw on the 2010–2019 VIRAC2 light curves, the infrared colours available from *WISE*, *Spitzer*-GLIMPSE, and VVV/VIRAC2, and a search for evidence for star formation activity within a 5 arcmin radius of each source using the SIMBAD data base and the *WISE* colour images (see Lucas et al. 2017, for details of the approach with these ancillary data).

The periods of the two AGB stars and the eclipsing binary (EB) were measured with the PDM2 code of Stellingwerf (Stellingwerf 1978), giving a very precise result in the case of the EB. Stim14 is listed as a microlensing event, based on visual inspection of the light curve for this isolated blue star. However, the event is not well sampled so this interpretation is not certain. The classification of the YSOs is secure in 8/10 cases. Only Stim2 and Stim12 lack firm evidence for location in a star formation region but their light-curve properties and the red $I1 − I2$ colours measured by *Spitzer*-GLIMPSE, support a YSO interpretation.

APPENDIX B: VVV LIGHT CURVES

This section presents the VVV/VVVX K_s light curves of the 38 sources observed in this work. The phase-folded light curves of periodic and quasi-periodic objects in our series are presented in Fig. B3. The VIRAC2 K_s light curves of the 61 spectroscopic confirmed YSOs, and the 5 post-main-sequence objects observed in this work are listed in Table B1. The infrared magnitudes, including J, H, K_s from VVV/VVVX, $W1$–$W4$ from *ALLWISE*, and $I1$ to *MIPS24* from *Spitzer* are presented in Table B2. Plots of the VIRAC2 light curves of the YSOs from Paper II are presented in Appendix C and are included in the online Supplementary info.

Table B1. VVV/VVVX VIRAC2 light curves for the full spectroscopic sample.

Name	GLON (deg)	GLAT (deg)	Observation time (MJD)	K_s (mag)	δK_s (mag)	χ-value
DR4_v5	307.318755	0.156974	55271.2096	14.16	0.01	1.0
DR4_v5	307.318755	0.156974	55271.2105	14.17	0.01	0.8
DR4_v5	307.318755	0.156974	55293.0966	13.51	0.25	1.5
DR4_v5	307.318755	0.156974	55293.0987	13.13	0.01	0.9
DR4_v5	307.318755	0.156974	55293.0990	13.15	0.02	1.0

Note. The full table is provided in the online supplementary files.

Table B2. Infrared magnitude of the 38 observed sources in this work.

Name	J	H	K_s	W1	W2	W3	W4	I1	I2	I3	I4	24 μm	α_{class}
v14	17.68	16.72	15.57	13.27	12.04	–	–	12.76	11.91	11.31	10.32	5.99	0.61
v16	16.14	14.70	13.65	11.54	10.56	6.74	–	11.76	10.84	10.14	9.10	6.21	0.07
v51	19.20	16.86	14.42	12.34	10.68	9.08	6.25	11.58	10.55	9.58	8.91	5.99	0.08
v53	17.78	–	14.54	10.98	9.65	7.72	–	11.47	10.05	9.27	8.39	4.96	0.61
v84	17.36	14.06	12.29	10.63	9.88	–	–	11.55	11.04	10.66	10.36	–	− 1.45

Note. J, *H* magnitude are from the 2010 multiband epoch of the VVV survey. The *J* and *H* magnitude of following sources are adopted from the 2015 epoch: v53, v319, v335, v389, v621, Stim5, DR4_v5, DR4_v10, DR4_v20, DR4_v34, DR4_v44, DR4_v67. The full table is provided in the online supplementary files.

Table B3. Information of spectroscopic observation.

Name	Observation date	Instrument	Slit Width (arcmin)	N_{exp}	t_{exp} (s)
v14	2017-05-31	FIRE	0.60	4	253.6
v16	2017-05-31	FIRE	0.60	4	158.5
v51	2017-06-01	FIRE	0.60	4	158.5
v53	2017-06-01	FIRE	0.60	4	253.6
v84	2017-06-01	FIRE	0.60	4	253.6

*Notes.*Details of spectroscopic observations.
N_{exp}: number of exposure. t_{exp}: exposure time.
The full table is provided in the online supplementary files.
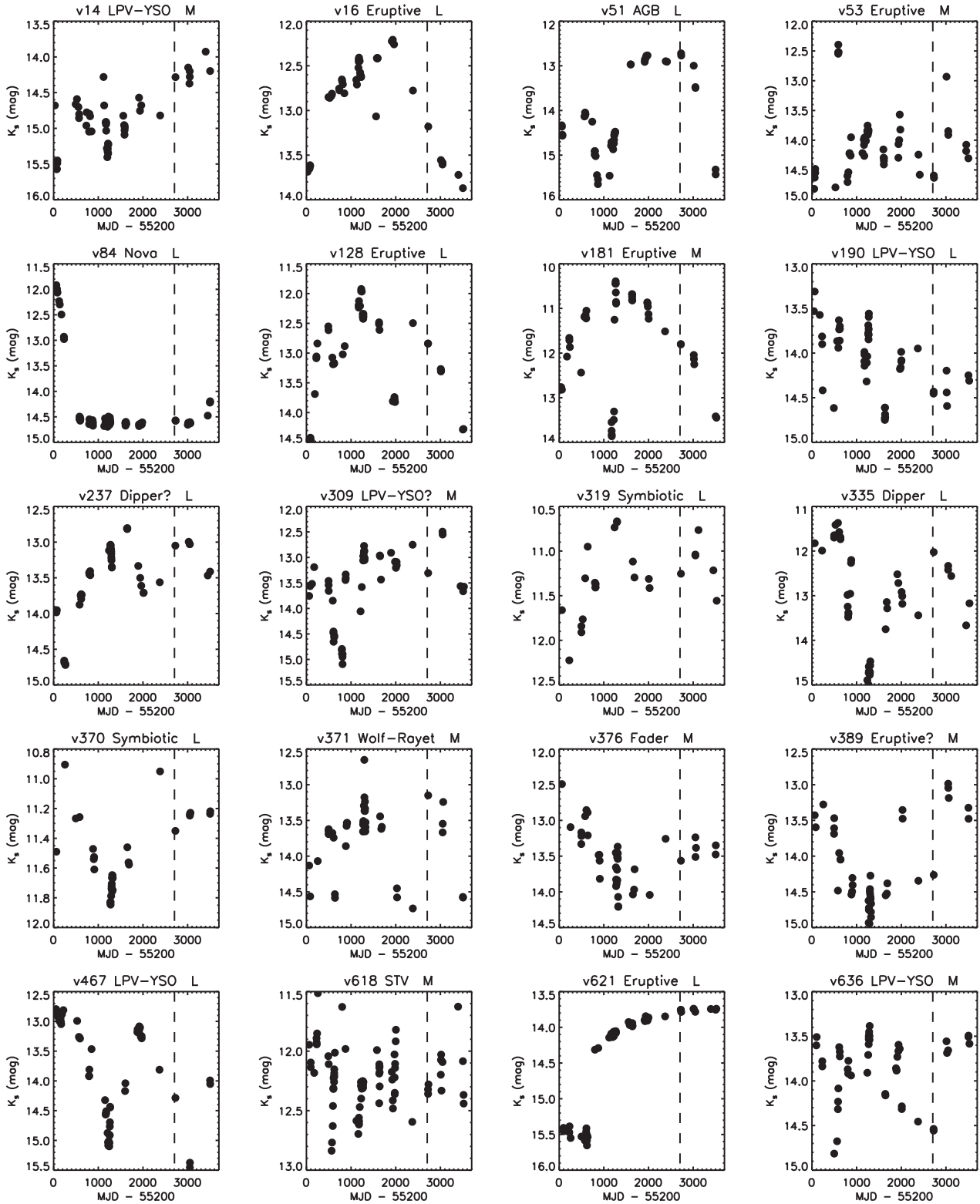
Figure B1. K_s-band light curves from the VVV survey. The variable classes listed in Table 1 are shown on the title of each plot. Vertical dashed lines mark out the observation time of spectroscopic epochs. The blue dots represent integrated K_s-band magnitudes from spectra taken in the 2019 epoch.
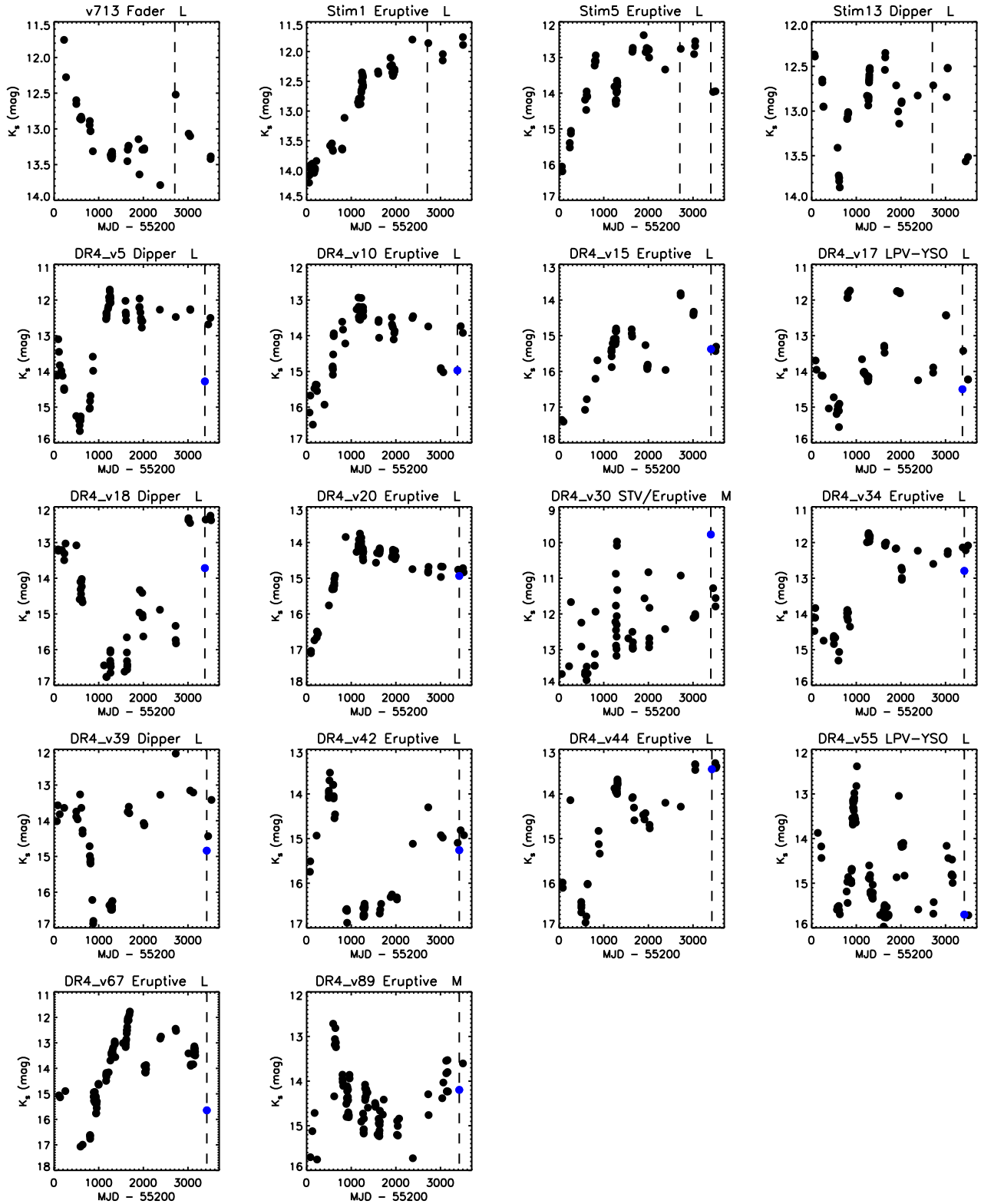
Figure B2. Fig. B1 continued.
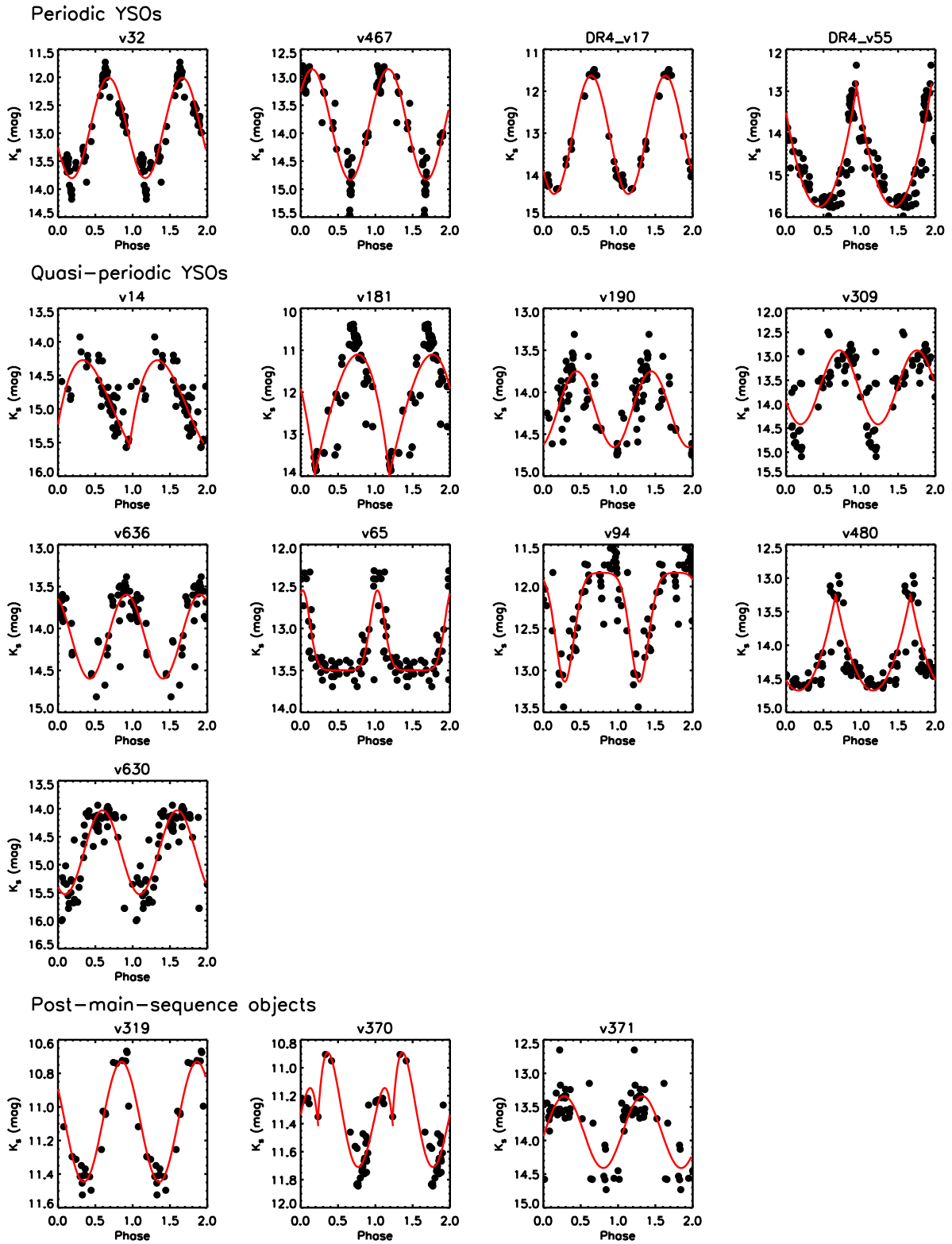
Figure B3. Phase-folded K_s-band VVV light curves of periodic and quasi-periodic objects found in this work. Analytical fitting curves are shown in red, including Gaussian (v65 and v94), polynomial (DR4_v55, v14, v480 and v370), and sinusoidal functions.

APPENDIX C: VVV LIGHT CURVES OF SOURCES OBSERVED IN PAPER II

[This section is available in the online supplementary material.]

APPENDIX D: 2MASS DATA FOR INDIVIDUAL SOURCES

[This section is available in the online supplementary material.]

APPENDIX E: THE MEASUREMENT OF EXTINCTION

[This section is available in the online supplementary material.]

APPENDIX F: YEAR-TO-YEAR VARIABILITY OF STIM5

[This section is available in the online supplementary material.]

APPENDIX G: AGB STARS AND SYMBIOTIC SYSTEMS: V51, V319, AND V370

[This section is available in the online supplementary material.]

APPENDIX H: SPECTRA OF 38 SOURCES OBSERVED IN THIS PAPER

In this section, we present the near-infrared spectra of the 38 sources observed in the 2017 and 2019 spectroscopic epochs (shown in Figs H1, H2, H3, H4, H5). The information of spectroscopic observation is listed in Table B3.
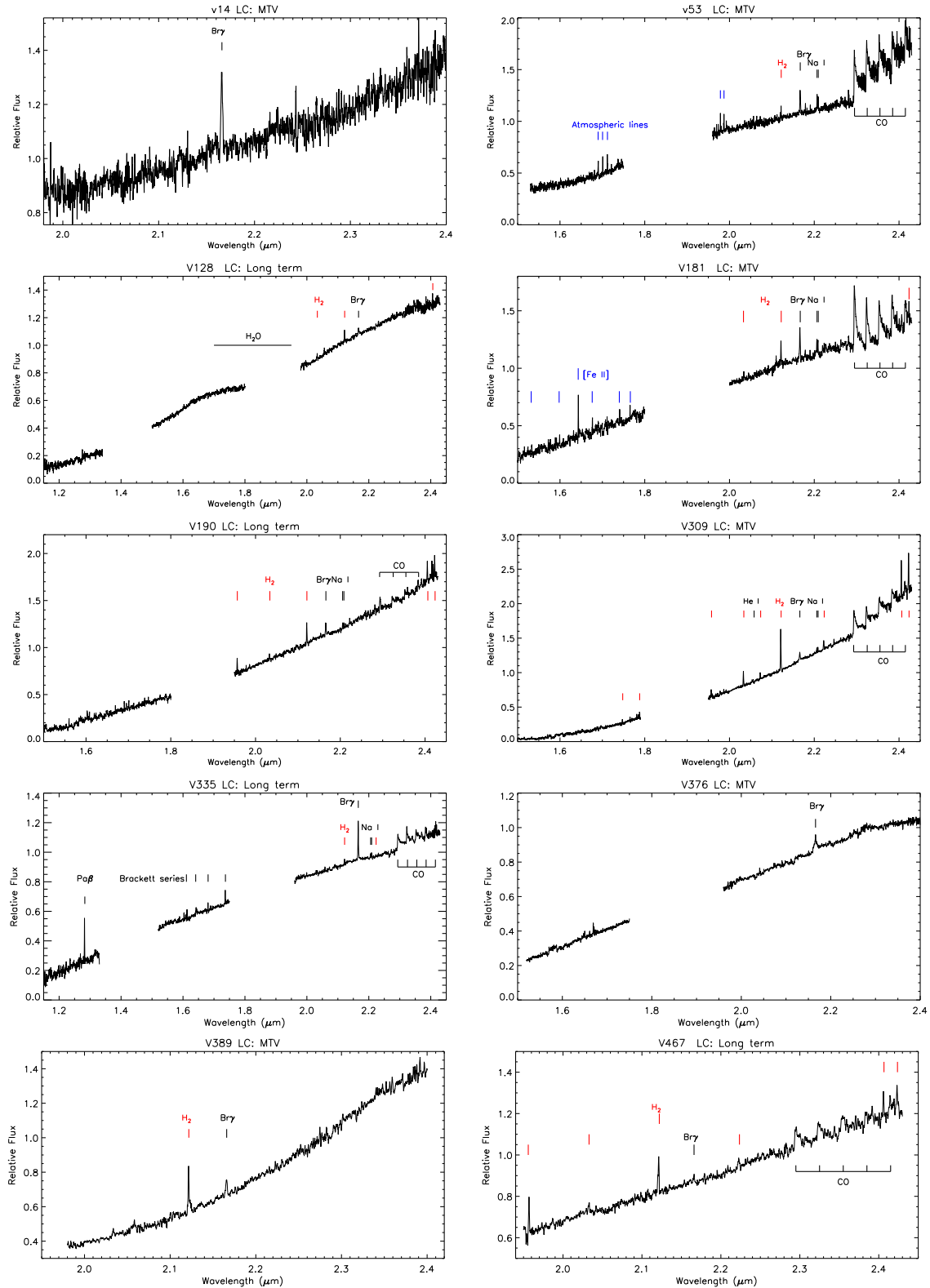
Figure H1. Near-IR spectra of emission-line YSOs observed in this work. These YSOs have signatures of magnetospheric accretion process. Spectroscopic features (e.g. molecular hydrogen emission, hydrogen recombination lines, sodium doublets, molecular bands) and atmospheric absorption regions are marked out on some plots as examples.
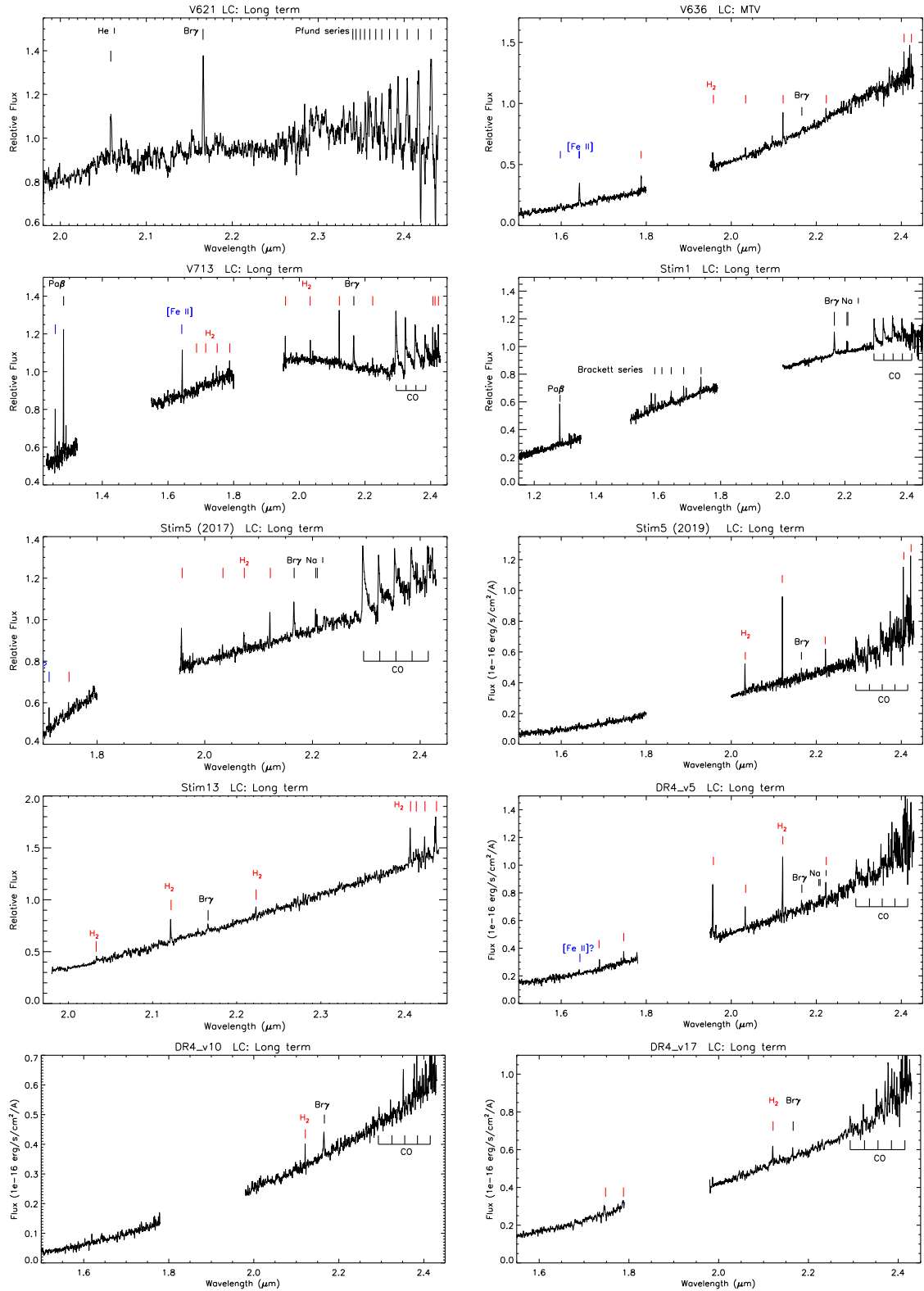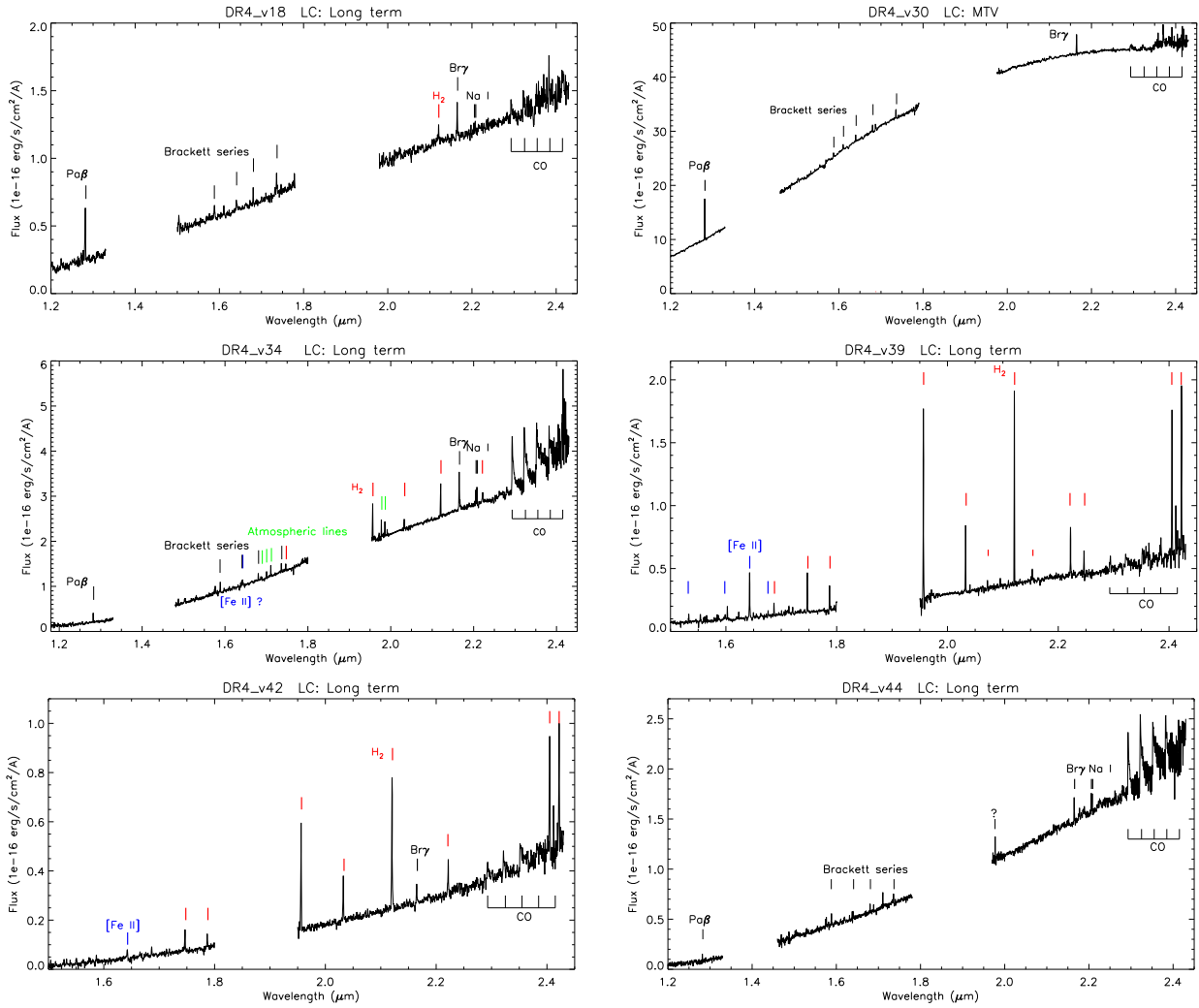
Figure H2. Fig. H1 continuued.

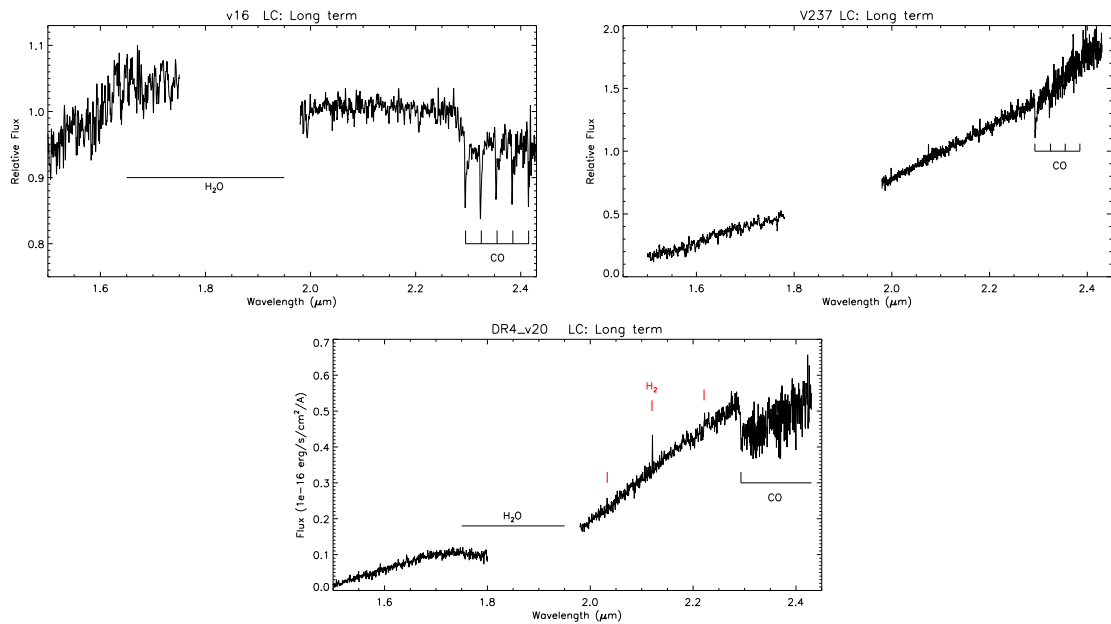**Figure H3.** Fig. H1 continnued.

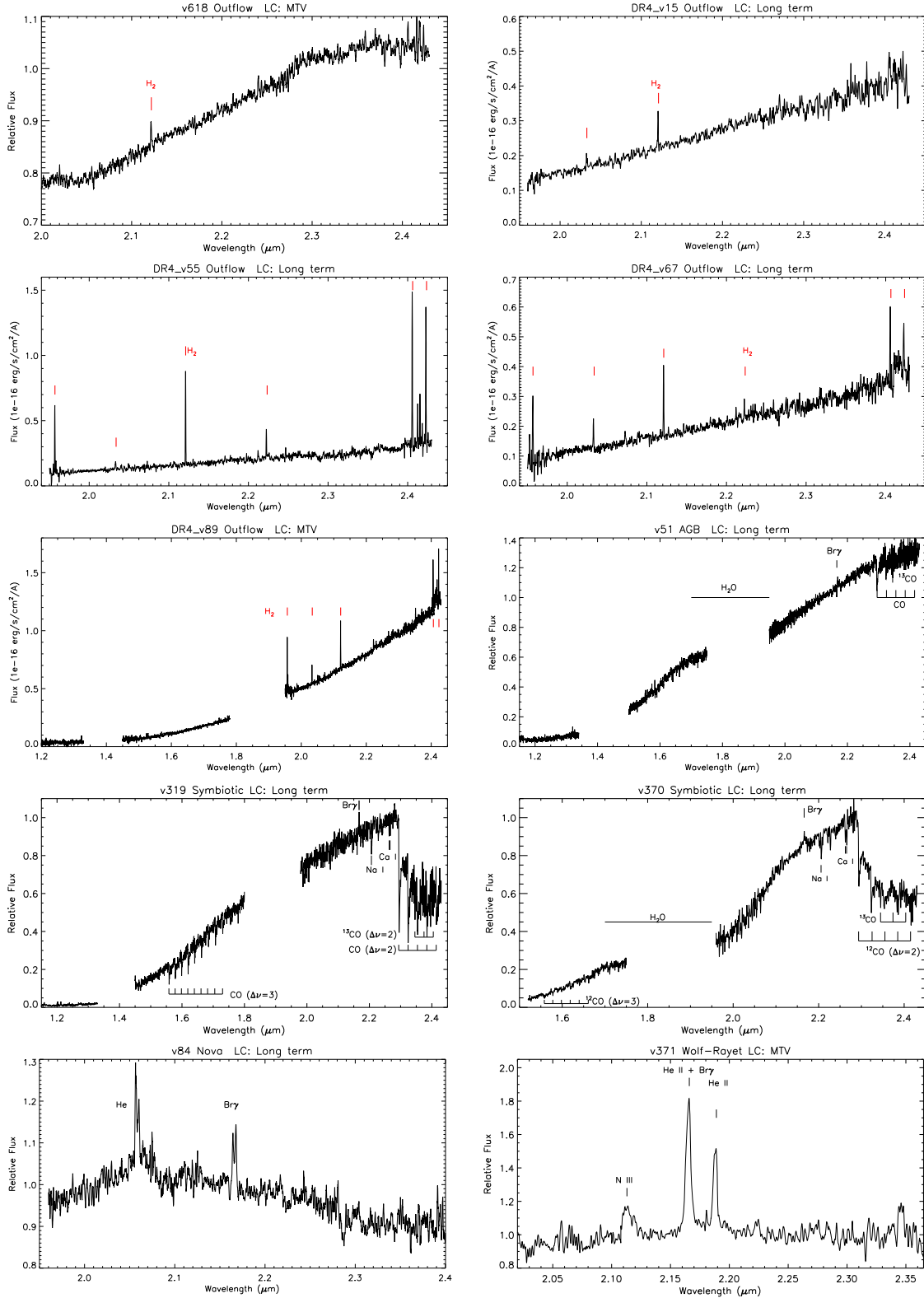**Figure H4.** Near-IR spectra of FUor-like YSOs with CO absorption features.

Figure H5. YSOs with outflow dominated spectra and post-main-sequence objects.

This paper has been typeset from a TEX/LATEX file prepared by the author.